University of Nevada, Reno

Voltage Control Strategies for Loss Minimization in Autonomous Microgrids

A dissertation submitted in partial fulfillment of the requirements for the degree of Doctor of Philosophy in Electrical Engineering

by

Mehdi Farasat

Dr. Andrzej M. Trzynadlowski/Dissertation Advisor

August, 2014

THE GRADUATE SCHOOL

We recommend that the dissertation
prepared under our supervision by

MEHDI FARASAT

Entitled

Voltage Control Strategies for Loss Minimization in Autonomous Microgrids

be accepted in partial fulfillment of the
requirements for the degree of

DOCTOR OF PHILOSOPHY

Dr. Andrzej M. Trzynadlowski, Advisor

Dr. Mehdi Etezadi-Amoli, Committee Member

Dr. M. Sami Fadali, Committee Member

Dr. Xiaoshan Zhu, Committee Member

Dr. Mehmet Gunes, Graduate School Representative

David W. Zeh, Ph. D., Dean, Graduate School

August, 2014

Abstract

This dissertation investigates the novel idea of flexible-voltage autonomous microgrids (MG), employing several interconnectable dc buses operating in a minimum-voltage mode. In comparison with the traditional fixed-voltage MGs, the proposed MGs reduce losses to gain significant enhancement in efficiency.

It is widely believed that energy systems of the future will heavily depend on MGs rich in power electronics converters (PECs). This dissertation is focused on MGs with a high degree of self-sufficiency, without precluding sporadic links with the power grid. Potential applications of those MGs include: (a) distributed generation power systems, (b) ships, land vehicles, aircraft, and spacecraft, (c) users in need of power supply impervious to vulnerabilities of the grid, and (d) localities lacking an access to a grid.

Modern pulse-width modulated PECs allow rapid and wide-range changes of voltages and currents. High switching frequencies result in high power quality and fast dynamic response, but each switching event causes energy loss related to the magnitudes of input voltage and output current. In the existing MGs, the bus voltages are maintained at a fixed level. However, many heavy loads, such as electric drives, operate most of the time with a reduced voltage, which is adjusted by decreasing the voltage gain of the feeding converter. This makes the voltage pulses high and narrow. If instead the pulses were made wide and low, then with the current unchanged the conduction losses would remain unchanged, but the switching losses would greatly decrease. This observation leads to the main idea of the dissertation, namely MGs whose dc-bus voltages are allowed to fluctuate

and which are maintained at the lowest possible level. Loss minimization, apart from energy savings, may be critical for autonomous MGs with a tight balance of power.

In this dissertation, two methods are proposed for calculating the minimum (optimum) required dc voltage level. In the first method, a central control unit allocates the minimum required dc voltages to individual buses by employing the information obtained from control systems of the adjustable voltage loads. For example, most of the variable-speed ac motors employ the so-called constant volts per hertz strategy, in which the relation between frequency and voltage is clearly specified. In the more sophisticated high-performance drives, the instantaneous values of the desired speed, torque, and current are available, allowing the required voltage estimation from the equation of power balance.
In the second method, the problem of determining the optimal dc voltage and power settings is formulated as an optimization problem with the objective function of minimizing the converter losses. Genetic algorithm is utilized in solving the optimization problem.

Due to limited available power from renewables, reducing the converter losses will enhance the survivability of the microgrid and ease the cooling requirements, resulting in a more compact system. A model of a 20-bus microgrid with the dc distribution network is employed to verify the effectiveness of the proposed methods.

ACKNOWLEDGEMENTS

First and foremost, I offer my gratitude to my advisor, Dr. Andrzej Trzynadlowski, for his guidance throughout my doctoral research. His positive support along with belief and patience led me to come up with this work. It was a great honor for me to pursue my research under his supervision.

I also wish to thank my advisory committee members, Dr. Mehdi Etezadi-Amoli, Dr. Sami Fadali, Dr. Xiaoshan Zhu, and Dr. Mehmet Gunes for their time, interest, and helpful comments.

I would like to express my deepest acknowledgement and love to my parents for their lifetime dedication, support and patience.

Last but not least, I thank my brother and sister for their invaluable support and encouragement.

Table of contents

List of Tables

List of Figures

Chapter 1

Introduction

Centralized power generation, unidirectional power flow, passive electricity distribution, and demand-driven operation are concepts coined more than one century ago when the first power systems were designed. In the last decades, modern solutions such as distributed generation (DG), mainly based on renewable energies, electrical energy storage (EES), flexible ac transmission systems, active demand management (ADM), microgrids (MGs), and smart control and management based on information and communication technologies (ICTs), have made it possible to plan new horizons for conventional power systems. However, not all the work necessary for planning the future power systems is concluded yet, and an intensive research effort must be conducted to make such advanced systems a reality [1].

MGs are usually defined as systems that have at least one distributed energy resource (DER), and which can form intentional islands in the electrical distribution system [2]. Typically an MG encompasses a portion of an electric power system located downstream of the distribution substation, and it includes a variety of DER units and different types of end-users of electricity and/or heat. DER units comprise distributed generation and distributed storage units with various capacities and characteristics [3]. The literature on MGs is abundant as MGs are amongst the most popular focus areas of today's power engineering research. The IEEE Xplore database includes over 1600 publications with

“microgrid” or “microgrids” in the title. Therefore, the subsequent review is limited to positions deemed representative for basic issues.

A systematic overview of different types of MGs is given in [4]. The technologies used in MGs, including distributed generation and storage, interconnection switches, and control systems, are described in [5]. Within MGs, loads and sources can be disconnected from, and reconnected to, the area or local electric power system with minimal disruption to the local loads [6]. The reorganization of a power system into units employing distributed energy resources and enjoying a certain degree of independence is explored in [7]. Regarding wider issues, three major benefits of MGs are specified as: (a) application of combined heat and power technology, (b) opportunities to tailor the quality of power delivered to suit the requirements of end users, and (c) the establishment of an environment favorable for increased energy efficiency and small-scale renewable generation investments. Key technical issues of MGs named in [8] are: renewable energy technologies, distributed generation, load control, and power electronic interfaces. A study of distribution system planning for high penetration of distributed generation is presented in [9]. It is shown that the operation of MGs leads to higher system reliability and makes it possible to simplify the structures of medium-voltage networks.

Economic and regulatory challenges of widespread MG deployment are explored in [10]. The economics of MGs is quite consistent around the world, with similar analysis methods emerging from more traditional areas of utility planning and project financing. The regulatory picture is more complicated, involving many different areas of public intervention. Hardware and control options for MGs are reviewed in [11]. The paper summarizes and highlights the operating principles and key conclusions of research and

field trials. An overview of MG demonstration projects in the US, Asia, and Europe is provided. An MG must provide several functions, such as the supply of electrical and/or thermal energy, participation in the energy market, specified service level for critical loads, black start subsequent to a failure, or provision for ancillary services. These objectives are achieved through either a centralized or a decentralized supervisory control [12]. Via the centralized control, the flow of MG-exchanged power with the host system is optimized in dependence on market prices and security constraints. A decentralized control approach provides the maximum autonomy for DER units and loads.

Control issues are widely covered in the reviewed literature. Typical operation of a central MG controller is described in [13]. The controller optimizes the output of local DERs and the power exchange with the main distribution grid. It is shown that MGs are economically beneficial, leading to either reduced energy prices for the consumers or to increased revenues for the aggregator. Under the multi-agent system strategy, a manufacturer of DER units or loads is allowed to embed a programmable agent in the controller of its equipment [14]. Thus, the required "plug and play" capability for installing future DER units and loads is ensured, although the installation of a new component requires extra programming of the central controller. An agent-based control framework for DER MGs is presented in [15]. To demonstrate the effectiveness of the proposed control, simulation studies have been performed on a dc distributed energy system that can be used in an MG as a modular power generation unit.

Reference [16] is mainly focused on the market participation of an MG. A control system capable of several integrated functions is proposed. Its architecture is based on the idea of "layered learning", where various controls and actions of the agents are grouped

depending on their effect on the environment. A novel approach, termed multi-agent reinforcement learning, has been introduced in [17] to increase the “intelligence” and efficiency of the controlled MG. The main advantage of the agents consists in their capability to learn and solve problems without the existence of a central controller. Typical structures of MGs and characteristics of the multi-agent systems are also described in [18]. The primary objective of the study was to test under real-life conditions control strategies for dispersed power systems. The proposed control system was implemented in a pilot MG of the Greek island Kythnos.

Regarding the interface with an MG, DER units are classified into two groups in [19]. The first group includes conventional rotary units that are interfaced with the MG through rotating machines. The second group utilizes PECs to provide coupling with the host system. Control strategies and dynamic behavior of an MG, particularly in the autonomous mode of operation, can be considerably different from that of a conventional power system. In contrast to the well-established operational strategies and controls of an interconnected power system, control and power/energy management strategies envisioned for an MG are mainly dependent on the DER technologies, load requirements, and operational scenarios.

It is pointed out in [20] that the majority of micro-sources to be installed in an MG are not suitable for direct connection to the electrical network due to the characteristics of the energy produced, such as the low-voltage dc power from fuel cells and PV arrays or high frequency ac power from microturbines. Therefore, a power electronic interface is required. The main functions of inverters interfacing MGs with the utility grid are voltage, frequency, and/or active/reactive power control. These functions can be divided

into grid-following and grid-forming controls. Each category can be further divided into non-interactive and grid-interactive strategies. The non-interactive grid-forming control is an explicit method for voltage and frequency control of a dispatchable unit in the absence of the utility grid. In the grid-connected mode, the objective of the inverter is to regulate the active and reactive power from the combo-source independently, while in the isolated mode the objective is to control the magnitude and frequency of the three-phase output voltage of the inverter [21].

A typical control scheme of an inverter presented in [22] consists of two cascaded control loops. The inner current control loops independently regulate the *d*-axis and *q*-axis components of the inverter output current in the rotating reference frame. The outer control loops regulate the power and voltage at the inverter output terminal. The results show that in an MG the dc and ac zones can be decoupled and separately controlled. An MG with both dc and ac links is proposed in [23] as an effective way to integrate a heterogeneous set of small-size DERs into the existing power infrastructure. The proposed approach uses a hierarchical framework with both dc and ac links to be implemented in the MG. A subset of basic DER units is first aggregated into a dc-bus link through dc/dc or ac/dc converters. The dc buses are then integrated into an ac-bus link through inverters, and the ac buses are integrated into an MG.

In [24], three possible control strategies, that is, PQ control, droop control, and frequency/voltage control of an MG are described. There exist many control schemes for load sharing based on the droop method, which has been extensively studied with respect to parallel ac-to-dc converters. However, less work has been done with respect to the resistive droop method in parallel dc-to-ac converters. In [25], a novel control scheme

improving the steady-state and transient response of parallel-connected non-communicating inverters is proposed. The controller has three nested loops: (a) an inner output-voltage regulation loop, (b) a resistive-output-impedance loop, and (c) a P/Q-sharing outer loop.

The voltage-power droop/frequency reactive-power boost control scheme, which allows current controlled voltage-source inverters (VSIs) to operate in parallel on the same MG, both in the island and on-grid modes is proposed in [26]. Each VSI has its own controller that sets its current references to regulate the voltage and frequency of the MG buses. In the island operation, multiple VSIs jointly regulate the MG voltage and frequency, and share common real and reactive loads in proportion to their voltage and frequency droop coefficients. In the grid-connected operation, the voltage and frequency are dictated by the grid. Another control method for parallel operation of inverters operating in an island grid or connected to an infinite bus is described in [27]. It is shown that controlling the active and reactive currents instead of the active and reactive powers exhibits certain advantages, especially in the short-circuit case. In [28], a PQ-controlled inverter is employed to supply required active and reactive powers. Using the voltage-source inverter control, specified values of voltage and frequency are maintained.

Reference [29] presents a control strategy for inverter-based sources that supports transitioning between grid connection and autonomous operation. The controller regulates the inverter terminal voltage and the active power delivered to the ac system using a phase-locked loop (PLL). The control method described in [30] employs nested feedback loops, with a transformation from *a-b-c* reference frame to *d-q*. The inverter current is controlled by the inner loop while the outer loop manages the voltage. Parallel

operation of multiple inverters can be controlled adding additional communication loops. A similar approach is described in [31]: the frequency is controlled by means of a PLL oscillator and the voltage in the island MG is regulated using a feedback loop. A control strategy for intentional islanding operation of MGs is provided in [32]. The method uses two control algorithms: one for on-grid operation and the other for the islanding. The instant at which the intentional islanding occurs must be detected in order to change the inverters mode from "grid-connected" to "intentional island". The islanding detection can be achieved using the synchronous reference frame PLL proposed in [33].

In [34], a dynamic model of an island MG is shown in a reference frame that is synchronized with the bus voltage. Based on the developed model, a supervisory control scheme is proposed. A proportional-integral (PI) controller sets the d-axis current reference to regulate the bus voltage magnitude, while a second controller sets the q-axis current reference to regulate the bus frequency. A survey of various features of MGs to compare the existent solutions and their potential limitations is given in [35]. The survey is focused on unplanned islanding detection techniques and control of inverters in the island MG.

Paper [36] proposes a method to control interfaces linking asynchronous ac power systems using back-to-back voltage-source converters. The dc bus voltage is controlled by a central PI controller which drives the power set point of each individual converter module. Several methods exist for power unbalance compensation. Control requirements regarding the compensation for a stand-alone MG are studied in [37]. The compensation is based on a dump load and a static compensator, which ensure the balance of the active and reactive powers. In order to compensate for sudden load fluctuations in an MG, the

electric double layer capacitors are investigated in [38], [39] as charge/discharge elements.

In [40], the MG is considered as an autonomous power system or a part of it, and transition between these two modes is analyzed. A novel neuro-fuzzy system stabilizer is proposed. A sliding mode control strategy for stability enhancement of MGs is presented in [41]. Simulation results show significant enhancement of dynamic performance of the MG. Both [40] and [41] show that with central control of MG based on variable-structure power system stabilizer there is no need for energy storage devices and load-shedding.

New control concepts are proposed in [42]. The primary control of each DER unit in the MG is augmented with secondary and tertiary controls. The primary control ensures stable operation of DERs, the secondary control minimizes the voltage and frequency deviations, and the tertiary control allows operation at an economic optimum. For optimal utilization of DERs, a novel idea of MGs based on a "dc energy pool" is outlined in [43]. The outputs of all DERs, both dc and ac, are converted into dc energy and fed to a dc-supply network. The dc-power consumers take energy directly from the network, while ac-power consumers use the dc-to-ac conversion using low-cost inverters. For energy balancing, energy storage devices are employed.

Near-term and long-term research directions in joint industry-academia projects for development of intelligent distributed MGs are presented in [44]. The emphasis is on distributed generation and distributed sensing strategies. Integration of intelligent MGs into the smart grid is proposed in [45] and [46]. Reference [47] provides review and assessment of basic control issues in MGs. Sizing of energy storage in MGs is analyzed in [48] and MG protection principles are described in [49]. Regulatory, commercial,

economic, environmental, and social issues are discussed in [50]-[53]. Finally, references [54]-[57] address the topics of isolated dc-bus microgrids and their voltage control, that is, those closest to the essence of the dissertation.

The dissertation is organized as follows: different types of distributed energy sources and power electronic interfaces in microgrids are discussed in Chapter 2. Classification of power electronic converters and their control are presented in Chapter 3. In Chapter 4, the idea of flexible-voltage operation and method to calculate minimum required dc-bus voltage is explained. Chapter 5 presents detailed description of voltage source converters operation and control and how they are embedded into ac-dc power flow equations. In Chapter 6, optimal power flow methods are reviewed, and voltage-power control of converters in the microgrid is formulated as an optimization problem. Chapter 7 presents the simulation results of the proposed control strategies on a 20-bus model microgrid with ac and dc buses. Conclusion and future work are discusses in Chapter 8.

Chapter 2

Power Electronics Interfaces in Microgrids

In this dissertation, dc distribution is assumed for autonomous microgrids (MG). The advantages of a dc distribution system over an ac one are discussed in Chapter 4. Fig. 2.1 depicts a typical MG with dc distribution lines.

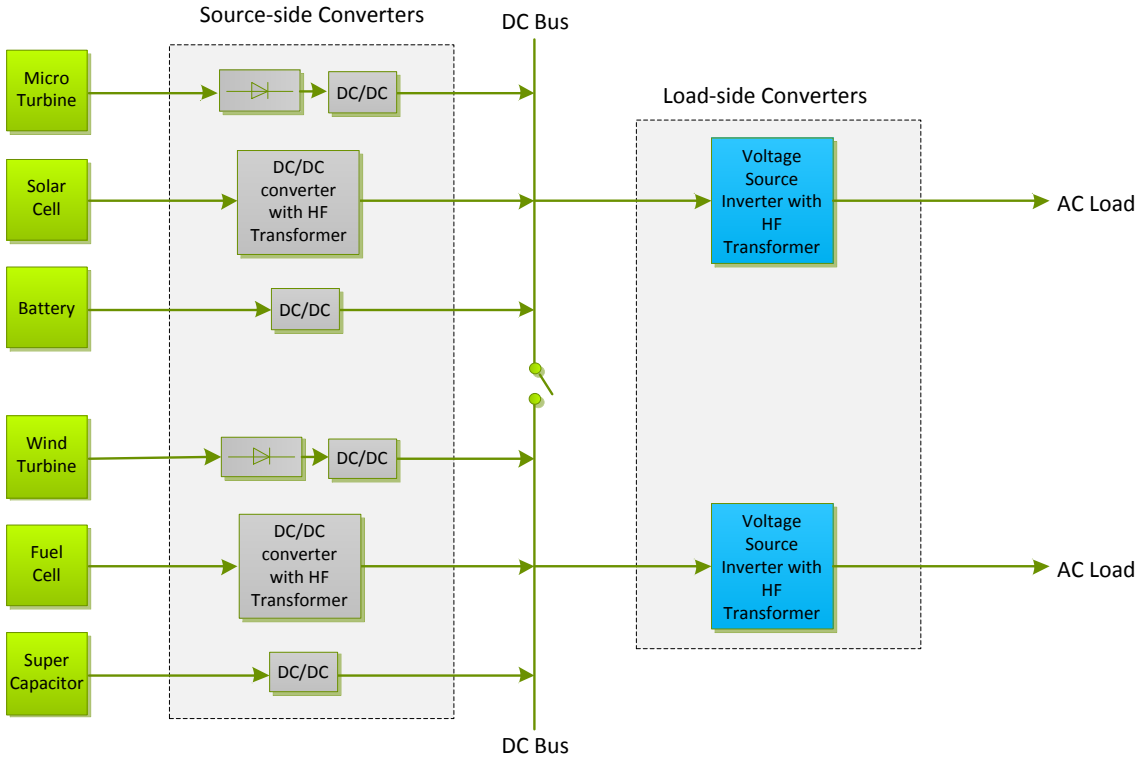

Fig. 2.1. Autonomous microgrid with dc distribution lines

The renewable sources are interfaced with the dc distribution network via power electronics converters (PEC), and ac loads are supplied through dc/ac inverters. Based on this configuration, PECs in MGs can be divided into two groups: source-side converters and load-side converters. Source-side converters interface the renewable energy resources

with the dc network. They are dc/dc or back-to-back ac/dc and dc/dc converters. If the renewable source generates dc output, dc/dc converters are employed as interfaces. Since the generated voltage is mostly at a low level, a boost converter is required to step up the voltage. On the other hand, if the renewable source generates ac output, an ac/dc converter is employed to convert it to dc, and a dc/dc converter boosts the voltage. Such an arrangement results from characteristics of the generated voltage. Most available renewable sources generate an output voltage variable frequency and amplitude, which is unsuitable for direct connection to the grid or loads. Therefore, an ac output voltage is first converted to dc voltage and then supplied to the loads through dc/ac inverters. Regulating the load voltage and frequency, in the island mode, and the active/reactive power delivered to the grid in grid-connected mode is carried out in the control scheme of the load-side inverters [2]. Chapter 3 is devoted to the state of the art in control of these converters in island and grid-connected modes. It should be noted that the proposed idea of flexible-voltage operation is aimed at maintaining the dc network voltage at the minimum possible level. Therefore, this concept is embedded in the control scheme of the source-side converters. Since the dc voltage level is reduced only at partial loads, the control system needs information on the voltage/power requirements of the variable voltage loads. Consequently, communication is required between the source-side and load-side converters in order to allocate the correct dc voltage level.

In the following subsections, a review of the available renewable energy technologies is given. The characteristics of the energy produced along with the required power electronics interfaces are explained. Next, a brief discussion on other advantages of PECs in MGs is presented.

2.1. Renewable Energy Sources

2.1.1. Photovoltaic Panels

Solar energy is captured by photovoltaic panels and converted to dc power. Since the produced power is of low voltage, a dc/dc boost converter is commonly required to interface the panels with the dc network.

2.1.2. Wind Turbines

Wind turbines are classified as horizontal- and vertical-axis turbines. Horizontal-axis turbines use a three blade rotor, while the vertical-axis ones use various shapes and numbers of airfoils. Due to higher efficiency and lower cost, horizontal-axis turbines are widely used in large-scale wind energy conversion systems.

Wind turbines can also be categorized as fixed-speed and variable-speed turbines. Fixed-speed turbines rotate at almost a constant speed and the highest efficiency is obtained at a specific wind speed, while conversion efficiency degrades at other speeds. They also require a sophisticated mechanical system in order to protect the blades from possible damages at high wind gusts. By contrast, variable-speed turbines are capable of operating at a wide range of wind speeds with high efficacy. Maximum power point tracking (MPPT) is commonly employed to adjust the turbine speed with respect to the wind speed. Thus, maximum wind power is captured and converted to electricity.

For variable-speed operation, a PEC is used to interface the generator coupled to the wind turbine with the grid/load. The significant advantages of employing a power electronics interface are increased efficiency, improved power quality, and reduced mechanical stress. The main disadvantage is the increased cost due to the usage of additional PECs. However, these costs are compensated for by the increased efficiency of

the generated power and less sophisticated mechanical systems. Thanks to the power electronic interfaces, large wind turbines have become feasible due to the reduced mechanical stresses on the turbine and the auxiliary structures. Based on these considerations, variable-speed wind turbines are dominant in the wind energy industry.

A wind turbine drives the shaft of an electric generator, which produces ac power. Therefore, an ac/dc rectifier must interface the generator with the dc network. The turbine is typically coupled to the shaft through a gearbox, which makes the generator rotate at a high speed and allows the generator to produce output voltage compatible with the grid voltage level. However, gearboxes are expensive and failure-prone, adding to the size, cost, and extent of maintenance of the system.

Current wind energy systems utilize three types of generators: squirrel cage induction generator (SCIG), doubly fed induction generator (DFIG), and synchronous generator (SG) (wound-rotor or permanent-magnet), with DFIG being the most common. The SCIG is low-cost and maintenance-free and mostly utilized in fixed-speed systems. The DFIG allows controlling the active power on the source-side and reactive power on the load/grid-side. Stator windings are directly connected to the grid, while the rotor is interfaced with the grid through a PEC. The cost of the power electronics interface is reduced as the converter only handles the rotor power, which is approximately 30 % of the rated power of the generator. The SG is commonly used in direct-drive wind energy systems. It features high efficiency and power density compared to wound rotor induction generator. As mentioned earlier, gearboxes degrade the reliability and increase the cost of the system. Therefore, direct-drive wind energy systems are popular in today’s market

[58]. However, the low-voltage at the generator output must be boosted up in the power electronics interface which is a challenging issue.

2.1.3. Fuel Cells

Fuel cells (FC) use hydrogen and oxygen and produce dc power (and water as a by-product). Various FCs are commercially available, such as phosphoric acid, solid oxide, and proton exchange membrane [59]. Since the output is a low voltage dc power, a boost dc/dc converter is required to interface FCs with the dc network.

2.1.4. Biomass

Biomass can be used directly to produce heat or converted to other forms of fuels like methane, ethanol and biodiesel. In the U.S. forest by-products such as wood residues are commonly used for generating electricity [60].

2.1.5. Geothermal Energy

Geothermal energy which is the heat from the earth is used to vaporize water or a fluid with low-boiling point. The produced steam spins a turbine coupled to the shaft of a synchronous generator which produces electricity. An ac/dc converter interfaces the generator with the dc network [60].

2.1.6. Ocean Energy

Two forms of energy, i.e., thermal and mechanical, are captured from the ocean. Similar to geothermal energy, the sun's heat on the surface of the water is used to vaporize a fluid with low-boiling point. The resulting steam rotates a turbine coupled to the shaft of a generator. Mechanical energy can be also captured from the tides and waves of the ocean and utilized in generating electricity [60].

Some renewable sources, such as wind and solar, have stochastic behavior and are therefore commonly used with energy storage devices. The surplus energy is stored during the off-peak loads and used at times when there is no wind or sunshine, or the load exceeds generation. Thus, a constant and stable output power is produced even under load fluctuations. The most commonly used energy storage devices are: batteries, ultra/super capacitors and flywheels. Ultra/super capacitors are suitable for short-term high-power applications, while flywheels feature fast response to power fluctuations compared to the other two devices. Therefore, they are finding more favor in supporting critical loads during grid interruptions [59]. Energy storage devices work with dc power. Since these devices store/inject power from/to the grid, bidirectional dc/dc converters are required to interface them with the dc network.

2.2. Advantages of Power Electronic Interfaces

In addition to the aforementioned advantages, PECs improve the power quality of MGs by controlling the harmonic content of the output voltage and current [59]. Several power electronics-based harmonic compensation systems have been proposed in the literature. Examples of such systems are active power filters, dynamic voltage restorers (DVR), or flexible ac transmission systems (FACTS).

PECs are also used to control the voltage and reactive power of distributed energy resources (DER). Modern PWM converters are capable of producing output waveforms with arbitrary amplitudes and phase angles. Therefore, they can operate at a wider power factor range compared to SGs and consequently control the flow of reactive power to or from the grid. Power electronics-based distributed sources can actively take part in regulating voltage and/or supply reactive power to the grid. However, in the grid-

connected mode, it is the grid that imposes the fixed voltage at the point of common coupling [59].

From its very beginning, semiconductor power electronics has been closely associated with adjustable speed drives. A typical drive comprises an electric motor fed from a PEC supplied from the grid or a battery. Consequently, research efforts in power electronics were mostly focused on single-input PECs, such as rectifiers and inverters, resulting in a high degree of technological maturity of those converters. However, in DERs, multi-input PECs can be employed to integrate several distributed sources and energy storage devices. Such systems, known as hybrid systems, have become feasible due to the recent advances in the power electronics technology [59].

Chapter 3

Classification of Power Electronics Interfaces in Microgrids

As mentioned in Chapter 2, the idea of flexible-voltage operation is applied in the control scheme of the source-side converters. In this chapter control of load-side converters in island and grid-connected modes are briefly reviewed. The presented discussions are based on [1] which gives a comprehensive review on the control of converters in ac microgrids.

3.1. Classification of Power Converters in Microgirds

3.1.1. Power Converters in Island Mode

In island mode, load-side inverters work similar to ideal ac voltage sources. Therefore, they can produce an output voltage with an arbitrary amplitude, E^*, and frequency, ω^*. Fig. 3.1 shows the control block diagram of a power converter in island mode. The controller uses two cascaded control loops working on the dq reference frame. The external loop controls the amplitude E^* of the voltage to be formed by the converter to match the grid voltage while the internal loop regulates the current injected by the converter. The other input to the control system is the frequency ω^* of the voltage to be formed by the converter.

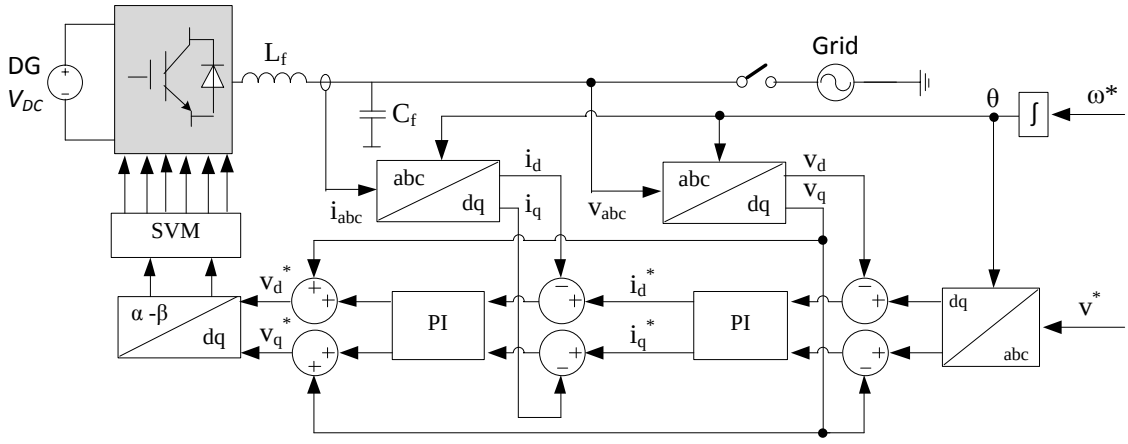

Fig.3.1. Control block diagram of a power converter in island mode [1]

3.1.2. Power Converters in Grid-Connected Mode

In grid-connected mode, the load-side converter can be employed to regulate the injected active and reactive power to the grid. In addition to power regulation, the amplitude and frequency of the converter can be controlled to match the grid voltage.

Fig. 3.2 shows control block diagram of a grid-connected converter for power regulation purposes. The inputs to the control system are active and reactive powers to be delivered to the grid. By controlling these quantities at a higher level, the converter controls the amplitude and frequency of the microgrid voltage. Reference active, P^*, and reactive, Q^*, power values are typically determined through MPPT.

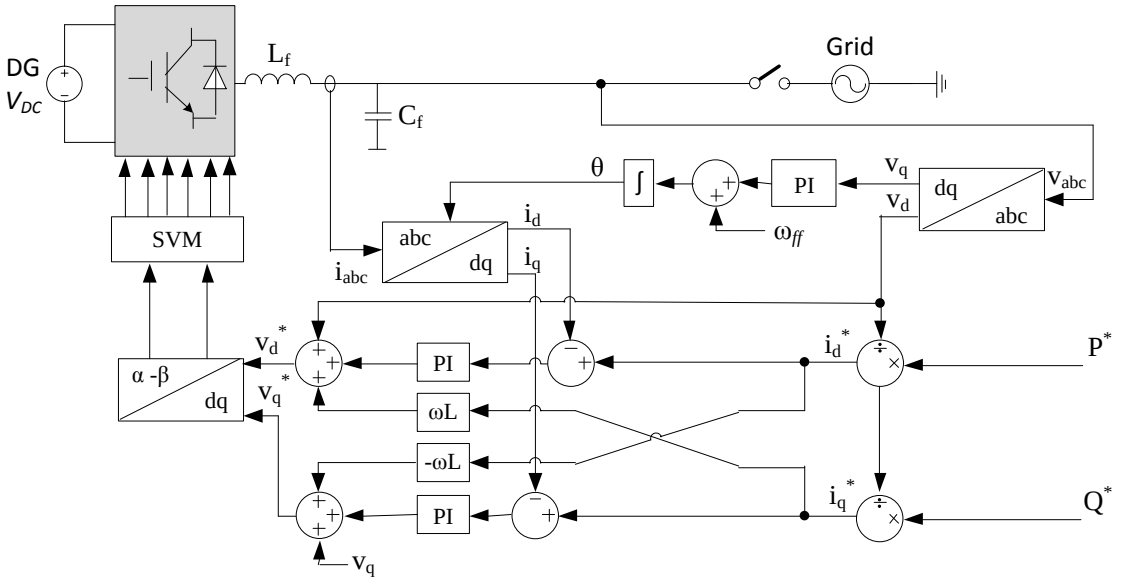

Fig.3.2. Control block diagram of a grid-connected converter for power regulation [1]

Fig. 3.3 (a) and Fig. 3.3 (b) depict a grid-connected converter controlled as a voltage source and as a current source, respectively. These control schemes provide both power and voltage regulation.

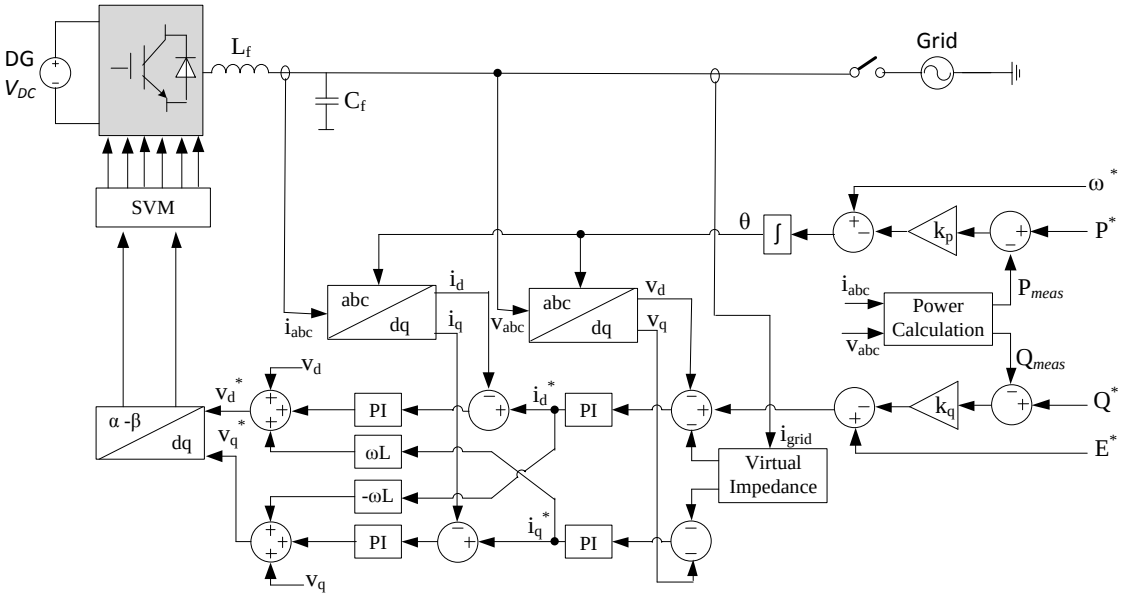

(a)

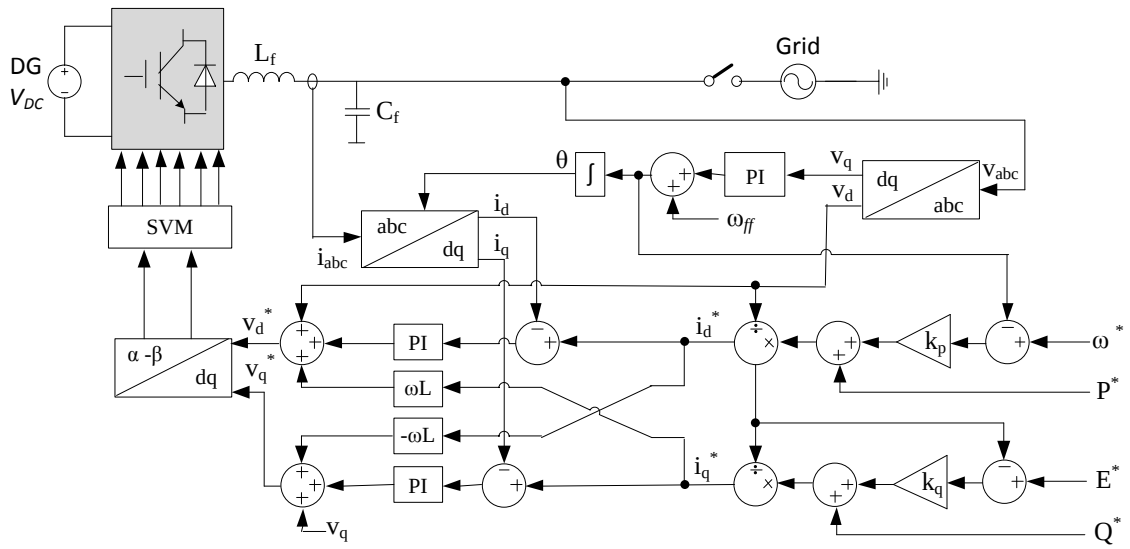

(b)

Fig.3.3. Control block diagram of a grid-connected power converter for power and voltage regulation, (a) Operation as a voltage-source, (b) Operation as a current-source [1]

3.2.Control Schemes of Power Converters in Microgrids

3.2.1. Power Converters in Island Mode

Fig. 3.1 shows the control block diagram of a power converter in island mode. There are two cascaded control loops: the external loop adjusts the output voltage of the converter, while the inner loop regulates the current injected by the converter to the grid. The external loop sets the current reference i^* to be injected by the converter to the grid by employing the error between the reference and the measured voltage. The inner current loop tracks the reference current set by the external voltage loop.

3.2.2. Power Converters in Grid-Connected Mode

As already mentioned, these converters employ two control loops in order to contribute in regulating the amplitude and the frequency of the grid and converter ac voltage. The inner control loop is a fast current control loop that adjusts the current to be injected into the grid by the converter. The external loop adjusts the reference current

such that a specific amount of power is delivered to the grid. The reference current is a feed-forward signal which is obtained from the reference powers, P^* and Q^* [61].

As seen in Figs. 3.1-3.3, PI controllers working on a dq synchronously rotating reference frame have been widely used in the control of power converters in microgrids. The controlled ac currents are transferred to the dq synchronously rotating frame by means of the Park transformation. Since the reference frame is synchronous with grid frequency, the currents are transformed to dc values. Two independent control loops are employed to regulate the $q-$ and $q-$axis current components. As mentioned earlier, the reference currents are typically provided by the external power control loop.

Fig. 3.2 shows the block diagram of a current control based on the dq synchronous reference frame. The grid voltage is provided as a feed-forward signal and a decoupling network is used to improve the performance of the controller. However, the performance of this control structure deteriorates under unbalanced grid conditions. The reason is the poor performance of PI controllers in regulating the transients that appear on the currents under faulty grid operation [61].

3.3. Droop Control

Since distributed generation sources and loads may be far away from each other, communication-based power sharing techniques are not suitable for grid-connected converters. Droop controllers are proposed as a solution to this problem. The droop controls are employed in grid-connected power converters. They control the grid voltage frequency and amplitude by adjusting the amount of delivered active and reactive powers. There is an analogy between the droop control and SGs in the grid-connected

mode. SGs also regulate the grid frequency and amplitude by adjusting the delivered active and reactive power, respectively.

Fig. 3.4 (a) depicts the equivalent circuit of a power converter controlled as an ideal voltage source connected to the grid through an interconnection line. Based on this configuration, the delivered active and reactive powers to the grid can be written as:

$$P_A = \frac{V_A}{R^2+X^2}[R(V_A - V_B cos\delta) + XV_B sin\delta] \tag{3.1}$$

$$Q_A = \frac{V_A}{R^2+X^2}[-RV_B sin\delta + X(V_A - V_B cos\delta)] \tag{3.2}$$

where P_A and Q_A are the active and reactive powers, respectively, V_A and V_B are the voltages of the converter and grid, respectively, δ is the phase shift angle between V_A and V_B, $Z = R + jX$ is the line impedance. Fig.3. 4(b) shows the phasor diagram of the equivalent circuit.

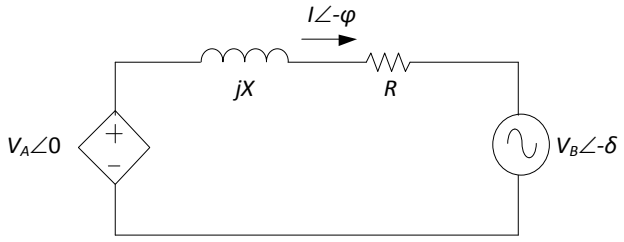

(a)

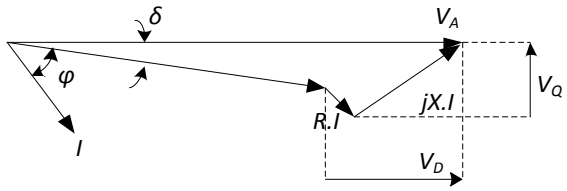

(b)

Fig.3.4. (a) Equivalent circuit of a power converter connected to an ac bus, (b) Equivalent space vector diagram [1]

Equations (3.1) and (3.2) show the relation between the delivered active and reactive power to the grid and the line impedance. Line impedance values vary in distribution and transmission networks. Therefore, different droop controls are employed in each case.

3.3.1. P/f and Q/V droop control

Table I [1] lists typical line impedance values in low, medium, and high voltage networks. The resistive component of line impedances in high- and medium-voltage networks are negligible compared to the inductive component. Therefore, neglecting resistance of the line will not have a significant effect on the power flow. Furthermore, due to small values of the power angle δ it can be assumed that $\sin(\delta) \approx \delta$ and $\cos(\delta) \approx 1$. Therefore, (3.1) and (3.2) can be rewritten as:

$$P_A \approx \frac{V_A}{X}(V_B sin\delta) \Rightarrow \delta \approx \frac{XP_A}{V_A V_B} \tag{3.3}$$

$$Q_A \approx \frac{V_A}{X}(V_A - V_B cos\delta) \Rightarrow V_A - V_B \approx \frac{XQ_A}{V_A} \tag{3.4}$$

TABLE I

Typical Line Impedance Values

Type of Line	R (Ω/km)	X (Ω/km)	R/X (p.u.)
Low Voltage Line	0.642	0.083	7.7
Medium Voltage Line	0.161	0.190	0.85
High Voltage Line	0.06	0.191	0.31

Equations (3.3) and (3.4) imply that the active power, *P*, depends on the power angle, δ, while the reactive power, *Q*, depends on the voltage difference, $V_A - V_B$. Therefore, the grid frequency and voltage can be regulated by adjusting the amount of active and reactive power injected to the grid, respectively. Based on these considerations, the following droop control equations are developed for inductive lines:

$$f - f_o = -k_p(P - P_o) \tag{3.5}$$

$$V - V_o = -k_q(Q - Q_o) \tag{3.6}$$

where f_o and V_o represent the nominal grid frequency and voltage, respectively, $P - P_o$ and $Q - Q_o$ are the deficit or surplus of active and reactive powers that must be injected by the converter to compensate for frequency and voltage deviations, and k_p and k_q are the slope of the frequency and voltage droop characteristics, respectively. Fig. 3.5 depicts the frequency and voltage droop characteristics. Therefore, *P/f* and *Q/V* droop characteristic set the active and reactive power reference values for each of the grid-connected power converters in order to have effective contribution in the regulation of the microgrid frequency and voltage [62].

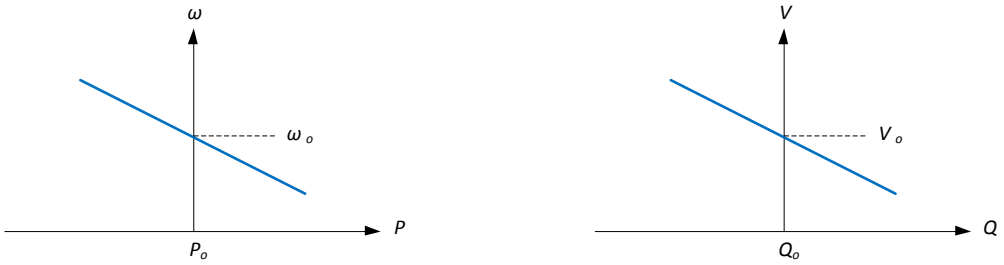

Fig. 3.5. *P/f* and *Q/V* droop characteristic [1]

3.3.2. P/V and Q/f droop control

As shown in Table I, the line impedance is more resistive in low-voltage networks. Therefore, the inductive component of the line impedance can be neglected without making any significant errors. Based on this consideration and assuming that δ is small, (3.1) and (3.2) can be rewritten as:

$$P_A \approx \frac{V_A}{R}(V_A - V_B cos\delta) \Rightarrow V_A - V_B \approx \frac{RP_A}{V_A} \tag{3.7}$$

$$Q_A = -\frac{V_A V_B}{R} sin\delta \Rightarrow \delta \approx -\frac{RQ_A}{V_A V_B} \tag{3.8}$$

Therefore, the injected active and reactive power controls the voltage amplitude and frequency in low-voltage networks. Based on these considerations, the following droop characteristics are developed for networks with resistive lines:

$$V - V_o = -k_p(P - P_o) \tag{3.10}$$

$$f - f_o = -k_q(Q - Q_o) \tag{3.11}$$

Fig. 3.6 depicts the *P/V* and the *Q/f* droop characteristics in grids with resistive line impedances [63].

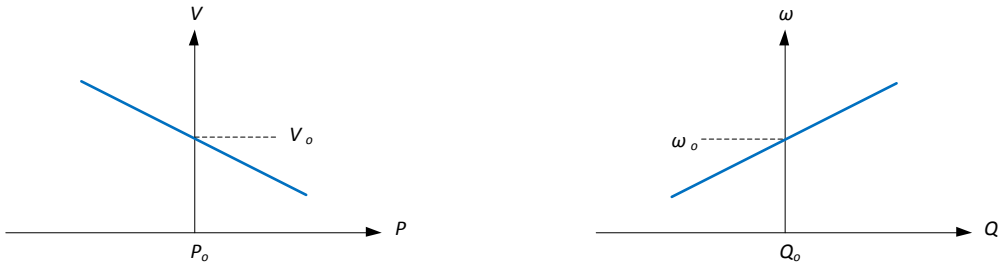

Fig. 3.6. *P/V* and the *Q/f* droop characteristics [1]

In [64], droop control equations are developed for the general case with resistive and inductive line impedance components. The active and reactive powers, P and Q, are transformed into the rotational power components, $\acute{P}$ and $\acute{Q}$, via matrix **T** as follows:

$$\begin{bmatrix}\acute{P}\\ \acute{Q}\end{bmatrix} = [\mathbf{T}].\begin{bmatrix}P\\ Q\end{bmatrix} = \begin{bmatrix}cos\varphi & -sin\varphi\\ sin\varphi & cos\varphi\end{bmatrix}.\begin{bmatrix}P\\ Q\end{bmatrix} = \begin{bmatrix}X/Z & -R/Z\\ R/Z & X/Z\end{bmatrix}.\begin{bmatrix}P\\ Q\end{bmatrix} \tag{3.12}$$

where $\varphi = \pi/2 - \theta = arctan(R/X)$ is the rotation angle of the matrix **T** and θ is the angle of the line impedance, $Z = Z\angle\theta$.

Applying rotation matrix **T** to (3.1) and (3.2) and assuming small power angle values, the following equations are obtained:

$$\acute{P_A} \approx \frac{V_A}{Z}(V_B sin\delta) \Rightarrow \delta \approx \frac{Z\acute{P_A}}{V_A V_B} \tag{3.13}$$

$$\acute{Q}_A \approx \frac{V_A}{X}(V_A - V_B cos\delta) \Rightarrow V_A - V_B \approx \frac{Z\acute{Q}_A}{V_A} \tag{3.14}$$

where $\acute{P}_A$ and $\acute{Q}_A$ are the rotated components of P_A and Q_A.

Equations (3.13) and (3.14) imply that the power angle and voltage difference can be controlled by regulating the rotating active power, $\acute{P}_A$, and the rotating reactive power, $\acute{Q}_A$, respectively. Consequently the droop control equations in networks with both resistive and inductive line impedance components can be written as:

$$f - f_o = -k_p(\acute{P} - \acute{P}_o) \tag{3.16}$$

$$V - V_o = -k_q(\acute{Q} - \acute{Q}_o) \tag{3.17}$$

The performance of the conventional droop control techniques depend on the accurate knowledge of the line impedance value. This calls for sophisticated grid impedance estimation techniques. Several solutions have been proposed to overcome this drawback. A basic solution is employing large inductors at the output terminals of power converters at the point of common coupling. In this way, inductive component becomes dominant in the line impedance value. However this adds to the size and cost of the system. Furthermore, a higher dc-bus voltage is required in order to compensate the voltage drop across the large inductor. This in turn results in reduced efficiency. A more effective solution was successfully implemented in [65-66], where adjustable virtual output impedance was used for power sharing among parallel inverters and limiting overcurrents under faulty grid conditions. The basic idea behind the virtual impedance is to modify the converter output voltage reference provided by the droop equations, v_{ref}^*, with respect to the virtual voltage drop across the virtual impedance:

$$v_{ref} = v_{ref}^* - Z_V . \boldsymbol{i}_{grid} \tag{3.18}$$

It should be mentioned that the value of the virtual impedance, Z_V, should be selected with respect to the line impedance value, Z. If Z_V is selected smaller than the line impedance, it will not have a significant effect in the power flow equations. Therefore, Z_V, should be larger than Z. Fig. 3.7 depicts the block diagram of the virtual impedance control in grid-connected power converters.

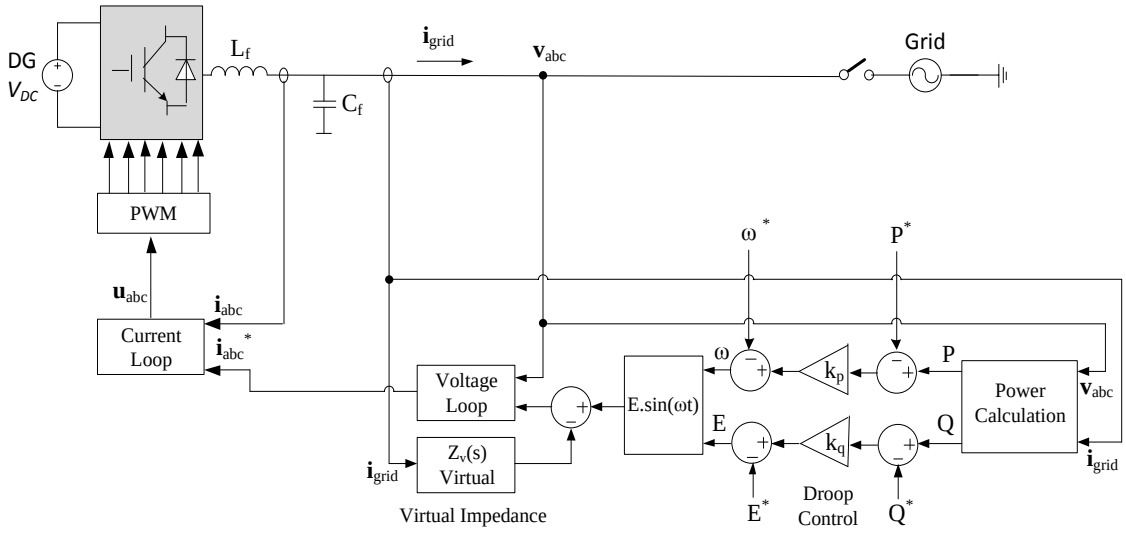

Fig. 3.7. Block diagram of the virtual output impedance control method [1]

Autonomous MGs of this dissertation are mostly controlled in the island mode and in a few cases in the grid-connected mode.

Chapter 4

Flexible-voltage Operation

Ship propulsion using an autonomous microgrid system is finding favor in many areas of the shipping industry. Most of the recent studies in the all-electric ship area are based on the notional medium-voltage dc (MVDC) shipboard power system (SPS) architecture dealt within the IEEE Standard1709-2010 [67]-[76]. The Standard addresses the main aspects of the MVDC shipboard distribution power systems. The MVDC architecture is expected to improve reliability, survivability, and power quality in SPS. The dc power distribution has several advantages over an ac one. According to [67] and [68] these include:

- simple connection and disconnection of different types and sizes of energy generation and storage devices
- reduction of size and ratings of the switchgear
- elimination of low-frequency transformers
- easy limiting and managing fault currents and enabling system reconfiguration
- weight reduction thanks to high-speed generators
- better exploitation of cables capability
- bi-directional power flow
- reduced fuel consumption thanks to variable speed prime mover operation

- high efficiency of energy storage and power conversion from batteries, fuel cells, and emergency generators
- no need for phase angle synchronization of sources and loads
- simple installation and operation of pulse loads.

4.1. Multi-Zonal MVDC SPS Architecture

A notional shipboard MVDC power system architecture as depicted in [67] is shown in Fig. 4.1. In this system, two main and two auxiliary generators (MTG1, MTG2, ATG1, and ATG2) feed a medium voltage dc ring bus operating at 5 kV through transformers and ac-dc converters. The dc power is distributed among five zones including the loads, VSCs, power conversion modules (PCMs), and power distribution modules (PDMs).

PCM1 steps 5000 V dc down to 800 V dc for dc zonal loads. The ac to dc conversion is carried out through PCM4s, which are commonly connected to the generators. On the other hand, PCM2 performs dc to ac conversion to supply ac zonal loads, such as the propulsion motor (PM).The architecture also contains energy storage devices, such as banks of capacitors or fuel cells, a pulsed load device, such as the charging circuit for a free-electron laser gun, and high power sensors, such as a radar array. In an MVDC system, the following settings must be pre-determined to maintain the dc voltage within desired margins: (I) the dc voltage reference setting for the VSCs operating in the voltage regulator mode, and (II) the optimal power reference settings of the remaining VSCs in the power dispatch mode [76].

In [69], a multi-agent system based load management technique has been proposed for all-electric ship (AES) power systems. The technique determines the optimal switch status of loads in the dc zones while satisfying the operating constraints of the system in real-

time. Kanellos *et al.* [70] propose an optimization methodology based on the sensitivity function for real-time solving the power management of SPS. In [71], the authors describe the rationale for the dc zonal system, characterize the stability issues, and discuss fault detection and load shedding problems. In [72], the SPS is reconfigured by optimizing the status of switches such that the maximum power is delivered to loads after the occurrence of a fault. In two companion papers, efforts are made in [73]-[74] to define voltage and frequency modulation constraints in ship electrical systems with pulsed loads. In [75], the voltage-power equations and control methods of voltage source converters (VSCs) are formulated, and the Newton-Raphson algorithm is employed to solve the power flow of a MVDC SPS containing multiple VSCs. The developed power flow is then used for security assessment.

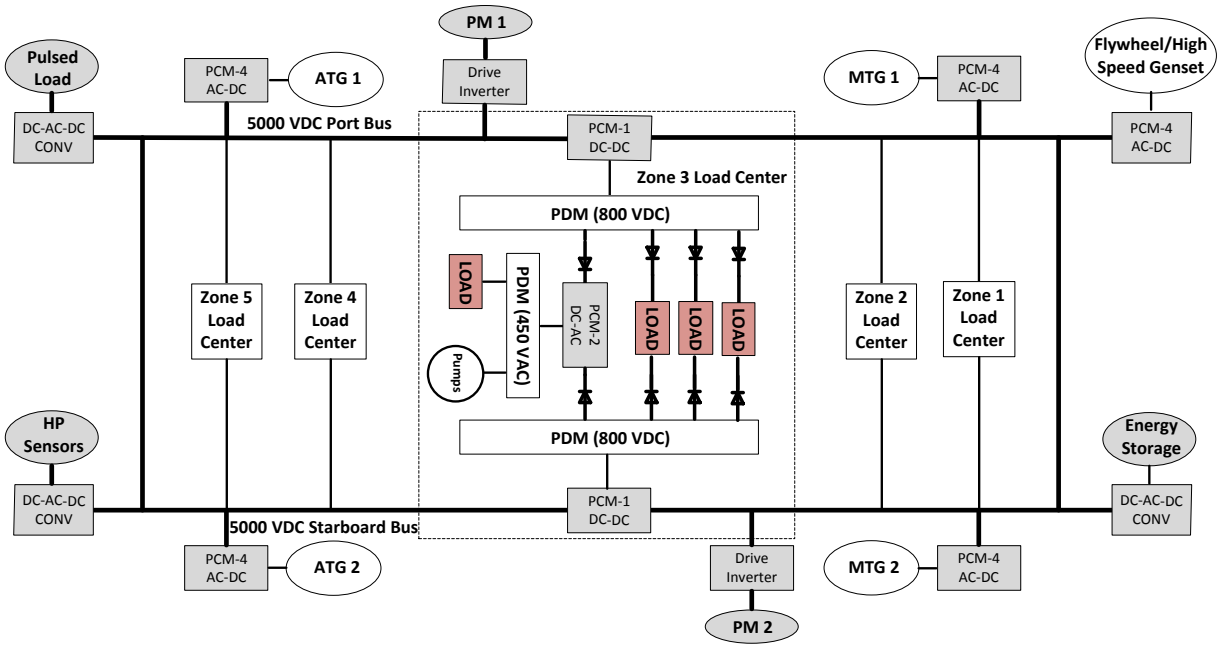

Fig.4.1. MVDC architecture of shipboard power system [76]

Research on MVDC SPSs has mostly focused on the system architecture and reconfiguration capabilities, stability conditions, power quality and power management. However, loss reduction in those systems has enjoyed much lower exposure in the literature. Therefore, this area calls for more research to achieve high efficient MVDC power systems. As pointed out in [67], converter losses are expected to be a dominant part of the overall losses in MVDC systems. Particular attention should be paid to reducing the losses in the system design, selection, and application. Voltage selection is also very important.

All VSCs suffer from an inherent conflict between high efficiency of power conversion and high quality of currents. The highly efficient square-wave mode of operation provides only coarse power conditioning with significantly distorted current waveforms. Therefore, most modern converters employ pulse width modulation (PWM) and their switches turn on and off with a relatively high frequency. Raising the switching frequency improves current waveforms but increases the switching losses. As a result, most existing PWM converters operate well below the frequency limits of modern semiconductor power switches. In addition to efficiency improvement, reduction of switching losses would ease the cooling requirements and result in greater compactness of the system, an especially vital concern in limited-space environments.

Several topologies and control strategies have been proposed in the literature to reduce converter losses [77]-[81]. In [77], two quasi-resonant dc-link (QRDCL) inverter topologies are discussed for “motor-friendly” application. An additional switch is added to the negative dc-link of the conventional QRDCL inverter, so that complete separation of the inverter from dc-link is possible. For the control of the inverters, a modified space-

vector pulsewidth modulation (SVPWM) is implemented, which requires two resonant cycles per switching period. A three-level zero-voltage switching (ZVS) dc converter for high input voltage and high output current applications is presented in [78]. Compared to the traditional topology, the proposed converter consists of additional center-tapped rectifiers and a series resonant tank to achieve ZVS turn-on for power switches and zero-current switching (ZCS) for rectifier diodes. A new modulation strategy based on an improved auxiliary resonant commutated pole (ARCP) inverter is presented in [79] to reduce the high commutation losses of the auxiliary commutation circuit (ACC) of ARCP inverters. Li *et al.* [80] propose a ZVS three-phase inverter in order to solve the hard-switching problem of the antiparallel diodes in the traditional six-switch three-phase inverter. The topology is modified by adding an extra switch and a new space vector modulation scheme is developed for the control of the inverter. In [81], a thorough analysis and calculation for the switching losses, current ripple, total harmonic distortion, and voltage spikes across the switching devices in a quasi Z-source inverter is presented for different switching sequences. Based on the carried out analysis, an optimized PWM sequence and a modified SVPWM technique for the inverter are proposed to achieve high efficiency of a hybrid electric vehicle motor drive.

To date, most research objectives are focused on modifying the switching strategies and/or achieving soft-switching to enhance converter efficiencies. The first solution leads to complicated switching techniques, while the second solution requires additional ACCs and switching devices which result in increased volume and cost of the converter. The idea of flexible-voltage dc bus proposed in this dissertation is aimed at addressing this

problem and at enhancing the autonomous microgrids, including MVDC SPS, by allowing the minimum-voltage operation.

4.2. Flexible-voltage Idea

The minimum voltage operation is similar to the state of hibernation into which certain species fall in winter to conserve energy. Hibernating animals experience depressed temperature - a thermal quantity formally analogous to voltage in the electrical domain. Recently, lowering the voltage supplying groups of transistors in computer CPUs has been proposed for applications in which the possible resultant inaccuracies would be non-catastrophic. The minimum-voltage operation should not be confused with the battery-saving "sleep mode" of such devices as laptops or cell phones.

Two basic rules of operation of an ac power grid are: (I) the demand and supply of real power must be balanced to maintain the nominal frequency, and (II) the demand and supply of reactive power must be balanced to maintain the nominal voltage. By extension, constant bus voltages and, in the case of an ac bus, a constant frequency, are assumed in most existing MGs. In contrast, the MG proposed here employs flexible-voltage dc buses whose voltages can fluctuate in a wide range.

To understand the idea of minimum-voltage operation of a flexible-voltage dc bus, note that the output voltage, V_o, of a PWM power converter can be written as

$$V_o = GV_i \tag{4.1}$$

where V_i denotes the input voltage and G is the adjustable gain (closely related to the modulation index), whose range depends on the type of the converter and the format of the input and output voltages. Assuming a dc output of the converter, the load can be

represented by its Thevenin equivalent circuit comprised of the EMF E_o, and resistance R_o. As E_o is a fraction of V_o, then

$$E_o = kV_o \tag{4.2}$$

where 0 <k< 1, and the load current, I_o, can be expressed as

$$I_o = \frac{(1-k)V_o}{R_o} \tag{4.3}$$

Eq. (4.3) can be generalized assuming that in the case of an ac load the phase shift between the EMF and output voltage is small. Then, the load resistance, R_o, can be replaced with a load impedance, Z_o, with I_o and V_o representing rms values of the respective quantities.

The switching-loss energy is a time integral of the switching-loss power, which is a product of current through the switch and voltage across the switch. The switching-loss energy depends on magnitudes of the input voltage and output current. Consequently, at a given switching frequency, the average switching loss, P_{sw}, also depends on those quantities, that is,

$$P_{sw} \sim V_i I_o = V_i \frac{(1-k)GV_i}{Z_o} = \frac{1-k}{Z_o} GV_i^2 \tag{4.4}$$

It can be seen from (4.4) that the dependence of switching loss on G is linear but that on V_i is square. For example, if the load voltage drops to a half of its maximum value, the supply voltage is also reduced by half, while the gain must increase by a factor of two. Consequently, as $2*(1/2)^2 = 0.5$, the switching losses decrease by 50% - a significant saving. Therefore, employing a minimum possible input voltage and a high gain is more efficient than constantly maintaining the high voltage required for full loads only. It is so because for a given fundamental voltage, low and wide voltage pulses result in lower

switching losses than high and narrow ones. It must be stressed that current levels will not be affected by the proposed approach to voltage control. Consequently, the conduction losses will remain unchanged.

A simple computer simulation illustrates the above conclusion. A three-phase inverter feeds an RL load of 15 Ω/ph. The turn-on time of the inverter switches is 0.5 μs and the turn-off time is 1.5 μs. Two cases of different supply dc voltages but of the same output line-to-line voltage of 230 V and 60 Hz were simulated. In the first case a 600V dc source was employed to supply the inverter. Next, the source voltage was decreased to 400 V. The corresponding values of the gain (equaling here the modulation index) were 0.54 and 0.81, respectively, and the switching frequency was set to 5 kHz. As seen in Fig. 4.2, the reduced supply voltage resulted in greatly reduced switching losses.

Flexible-voltage MGs will be most practical in arrangements in which the bulk of the power is delivered to loads often operating with a reduced voltage, such as electric drives or HVAC systems. Note that most engineering systems operate on full load rather infrequently. Loads requiring fixed ac voltage, such as computers or lighting, would have to be supplied from a separate ac bus. Propitiously, those loads typically consume much less power than most of the variable-voltage loads.

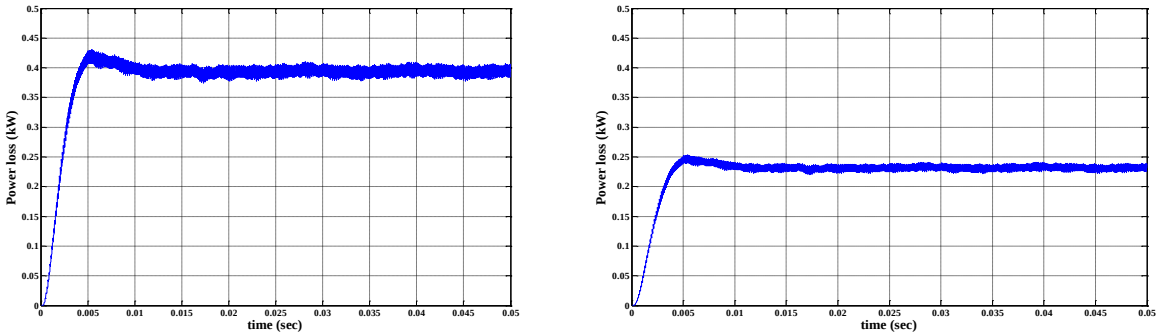

Fig. 4.2. Switching losses in simulated inverter. Left: V_i = 600 V, G = 0.54, right: V_i = 400 V, G = 0.81.

A flexible-voltage MG contains two groups of VSCs: the source-bus and bus-load ones, subsequently referred to as source converters and load converters, respectively. Voltage rating of these converters depends on the highest value of their input and output voltages. The input voltage of a source converter is imposed by the given source and the output voltage of a load converter by requirements of the given load. Hence, the related voltage ratings are independent of the bus voltage. On the other hand, the bus voltage equals the output voltage of source converters and the input voltage of load converters. Consequently, voltage ratings of these converters can only be impacted by the highest bus voltage, which is the same in the fixed- and flexible-voltage SPSs. It can thus be concluded that voltage ratings of all MG converters do not depend on the bus voltage control mode. The same observation applies to the current ratings of load converters, which are impressed by specific loads.

The proposed MGs may not be more expensive or less reliable than the traditional fixed-voltage ones. Therefore, converter sizing and protection schemes require special attention. The idea of flexible dc bus voltage may create an impression that in order to deliver a given amount of power to the loads, the current drawn from the sources must increase when the bus voltage decreases. This is a false conclusion because when the

maximum load power is needed the highest bus voltage is set up. The basic idea of the minimum-voltage operation is that the reduced load voltage of the load converter, which in the fixed-voltage MGs is produced by a corresponding reduction of the gain, *G*, can also be obtained with the maximum *G* and a reduced bus voltage. Denoting the rms load voltage by V_L, the amount of power in practical loads is proportional to V_L^n, where *n* is contained within the range of 1 (when the load current does not depend on V_L) to 2 (when the load does not contain an EMF). Therefore, the reduced bus voltage corresponds to the load power that is reduced in the same degree or more. Thus VSCs in the flexible-voltage MG will have the same voltage and current ratings at those in an equivalent fixed-voltage MG, whose bus voltage equals the highest bus voltage in the flexible-voltage case.

The voltage-related protection schemes of the flexible-voltage MG will certainly differ from those of fixed-voltage MGs. Collapse of the bus voltage in the latter MG indicates a serious failure of the system. Here, precautions must be taken to distinguish between such a collapse and a decrease of the bus voltage resulting from the minimum-voltage operation of the MG. This can be accomplished by notifying the protection system by the control system of the incoming reduction of the bus voltage just before the actual change. As currents are unaffected by the proposed bus voltage control, the current protection schemes will remain the same as those employed in MGs with fixed bus voltage.

4.3. Effect of Flexible-Voltage Operation on Power Losses

Fig. 4.3 depicts the forced commutation process in a semiconductor power switch during a switching cycle. In general terms, the conduction loss of a semiconductor switch equals the voltage drop across the device (V_T) multiplied by the current flowing through

it. Under the same load, the conduction losses will be same in both fixed-voltage and flexible-voltage operation because of same switches and current levels in both cases. On the other hand, the switching losses depend on the time integral of the switching loss power and switching frequency. The turn-on, t_{on}, and turn-off, t_{off} , time periods may vary from one semiconductor to another. For example, GTOs have longer tail currents, which result in much longer turn-off times compared to MOSFET's or IGBT's. On the contrary, the turn-on time of a GTO is shorter than that of an IGBT. However, employing a reduced voltage level, V, will reduce the time integral of turn-on and turn-off power losses regardless of type of the semiconductor power switch. In a two-level VSC, $V = V_{dc}$. Consequently, flexible-voltage operation can effectively reduce the switching losses of any forced commutated semiconductor switch.

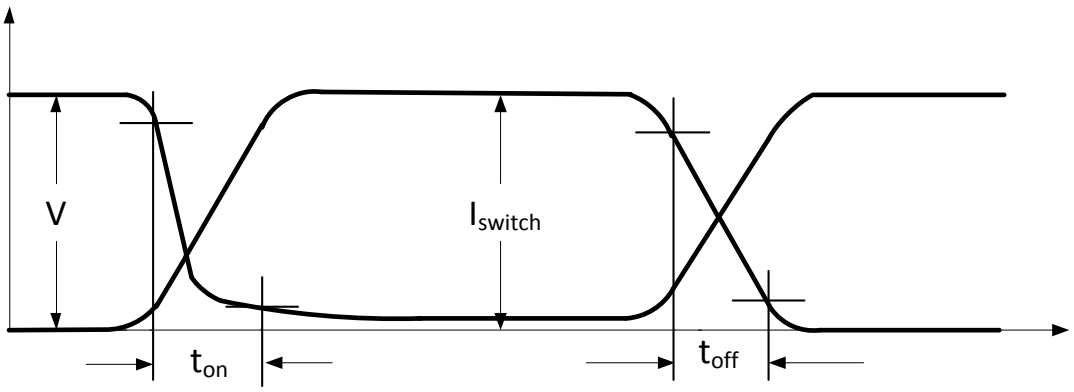

Fig. 4.3. Commutation process (off-on-off) in a semiconductor power switch during a switching cycle

In the following subsections, analytical switching and conduction losses of IGBT and GTO devices are investigated, and the effect of flexible-voltage operation on these losses is discussed.

4.3.1. GTO

The conduction loss of the GTO thyristor, $P_{C,GTO}$, can be obtained as [82]

$$P_{C,GTO} = J.\frac{E_g}{q} + J.\frac{3\pi}{8}.\frac{kT}{q}.e^{\frac{3V_B}{2L_aE_C}} \tag{4.5}$$

where J is anode current density, E_g is energy bandgap at room temperature, q is electron charge, $\frac{kT}{q}$ is thermal voltage, V_B is breakdown voltage, L_a is ambipolar diffusion length, and E_C is avalanche breakdown electric field. In Eq. (4.5), the first term is the loss to overcome the junction voltage barrier, and the second term is the loss across the lower base region. Under flexible-voltage operation, it is expected that the conduction loss will remain without changes because of same load current and physical characteristics of the device.

The turn-on and turn-off processes of the GTO thyristor can be divided into two parts, respectively. For the turn-on process, the depletion layer capacitance needs to be discharged first. Then the anode current injects charges into the drift region until GTO enters its latching state. Hence, the turn-on power dissipation of the GTO thyristor is given by [82]

$$E_{on,GTO} = \frac{1}{3}\varepsilon E_C V\left(\frac{V}{V_B}\right)^{0.5} + J^2\frac{3\tau_a V_B^2}{\varepsilon\mu_n E_C^3} + \frac{E_g}{2q}J\tau_a \tag{4.6}$$

where ε is the permittivity of the semiconductor, V is the applied voltage, τ_a is ambipolar carrier lifetime, and μ_n is electron mobility. During the turn-off, the entire anode current flows to the gate electrode. Once the voltage reaches the clamped voltage value, the current drops to a lower level and is followed by a long current tail. Therefore,

$$E_{off,GTO} = \frac{1}{2}\frac{\varepsilon E_C V}{1-\alpha_{npn}}\left(\frac{V}{V_B}\right)^{0.5} + VJ\tau_a\alpha_{npn,max} \tag{4.7}$$

Here, $\overline{\alpha_{npn}}$ and $\alpha_{npn,max}$ are the average and maximum current gains during the voltage rise phase, respectively [82]. Equations for calculating L_a, τ_a, μ_n, $\overline{\alpha_{npn}}$ and $\alpha_{npn,max}$ are given in [82]-[83]. The switching power loss can be then calculated as

$$P_{sw} = \left(E_{on,GTO} + E_{off,GTO}\right).f_{sw} \tag{4.8}$$

As can be concluded from (4.7) and (4.8), the turn-on and turn-off energy losses depend on the applied voltage, $V(=V_{dc})$. Therefore, a reduced dc-bus voltage will effectively reduce the energy losses, and consequently, the switching power loss in the GTO thyristor.

4.3.2. IGBT

The following equation expresses the switching losses of a VSC with sinusoidal ac line current and IGBT switches [84]:

$$P_{sw} = \frac{6}{\pi}.f_{sw}.\left(E_{ON,I} + E_{OFF,I} + E_{OFF,D}\right).\frac{V_{dc}}{V_{ref}}.\frac{\hat{I}_L}{i_{ref}} \tag{4.9}$$

where f_{sw}denotes the switching frequency, $E_{ON,I}$, $E_{OFF,I}$ are the turn-on and turn-off energies of the IGBT, respectively, $E_{OFF,D}$ is the turn-off energy of a diode due to the reverse recovery charge current, V_{dc} is the dc link voltage, and $\hat{I}_L$ is the peak value of ac load current. The switching energies provided by the data sheets are given for a certain reference voltage, V_{ref}, and are equal to the blocking state voltage of the IGBT occurring before the corresponding commutation and a reference current, i_{ref}, which is the on-state current after this commutation. As elaborated in [85], the turn-on and turn-off losses in IGBT and diode power modules increase when the temperature, load current, or dc

voltage increase. Based on these considerations, it can be seen from Eq. (4.9) that low dc bus voltage reduces switching losses.

In contrast to switching losses, the conduction losses directly depend on the modulation function that is used. With knowledge of the relevant modulation function, the conduction losses of a single IGBT, P_{CT}, and a diode, P_{CD}, can be expressed by

$$P_{CT} = \frac{u_{CE0}\hat{I}_L}{2\pi}\int_0^{\pi} \sin(\omega t).\frac{1+F(t)}{2}d\omega t + \frac{r_C\hat{I}_L^2}{2\pi}\int_0^{\pi} \sin^2(\omega t).\frac{1+F(t)}{2}d\omega t \quad (4.10)$$

$$P_{CD} = \frac{u_{D0}\hat{I}_L}{2\pi}\int_0^{\pi} \sin(\omega t).\frac{1-F(t)}{2}d\omega t + \frac{r_D\hat{I}_L^2}{2\pi}\int_0^{\pi} \sin^2(\omega t).\frac{1-F(t)}{2}d\omega t \quad (4.11)$$

where ω is the load current angular frequency, $F(t)$ is the modulating function, u_{ce0} and r_c are the threshold voltage and differential resistance of the IGBT, u_{D0} and r_D are threshold voltage and differential resistance of a diode, respectively. These parameters can be calculated from the I-V characteristic curves provided in the data sheet [86]. The modulating function is a sine wave for carrier based sinusoidal PWM, i.e., $F(t) = M.sin(\omega t)$. In case of SVPWM this function is defined as

$$F(t) = M.sin(\omega t) + \frac{3\sqrt{3}}{8\pi}\sum_{k=0}^{\infty}\left(\frac{sin(3(4k+1)\omega t)}{18k^2+9k+1} - \frac{sin(3(4k+1)\omega t)}{18k^2+27k+10}\right) \quad (4.12)$$

For the chosen PWM techniques, equations (4.10) and (4.11) turn into

$$P_{CT} = u_{ce0}\hat{I}_L\left(\frac{1}{2\pi} + \frac{M\cos\phi}{8}\right) + r_c\hat{I}_L^2\left(\frac{1}{8} + \frac{M\cos\phi}{3\pi} + 2\pi F_{SVM}\right) \quad (4.13)$$

$$P_{CD} = u_{D0}\hat{I}_L\left(\frac{1}{2\pi} - \frac{M\cos\phi}{8}\right) + r_D\hat{I}_L^2\left(\frac{1}{8} - \frac{M\cos\phi}{3\pi} - 2\pi F_{SVM}\right) \quad (4.14)$$

Here, M is the modulation index and ϕ is the displacement angle between the fundamental of the modulation function and the load current. In case of SPWM, F_{SVM} equals zero. For SVPWM, F_{SVM} can be expressed by:

$$F_{SVM} = \frac{6\sqrt{3}}{\pi}\sum\left(\frac{cos(k\phi)}{k^5-5k^3+4k} - \frac{cos(l\phi)}{l^5-5l^3+4l}\right); l = 3(4v+1); k = 3(4v+3); v = 0,1,2,\ldots \quad (4.15)$$

It should be noted that the value of F_{SVM} is very low when compared to the total conduction losses. Therefore, the conduction losses for SVPWM can be computed in the same way as for SPWM with only a minor loss of accuracy [84].

As explained earlier, the flexible-voltage operation will have no effect on the load current or the power factor, but will result in higher modulation indices and wider PWM pulse widths. Therefore, to explore the effect of flexible-voltage operation on the conduction losses, two cases with the same load current, $\hat{I}_{L_1} = \hat{I}_{L_2} = \hat{I}_L$, and power factor, $(\cos\phi)_1 = (\cos\phi)_2 = \cos\phi$, but with different modulation indices, M_1 and M_2, where $M_2 > M_1$, can be considered. Under these circumstances, the IGBT conduction losses will increase by

$$\Delta P_{CT} = (P_{CT})_2 - (P_{CT})_1 = u_{ce0}\hat{I}_L\left(\frac{(M_2-M_1)\cos\phi}{8}\right) + r_c\hat{I}_L^2\left(\frac{(M_2-M_1)\cos\phi}{3\pi}\right) \quad (4.16)$$

On the other hand, the diode conduction losses will decrease by

$$\Delta P_{CD} = (P_{CD})_2 - (P_{CD})_1 = -u_{D0}\hat{I}_L\left(\frac{(M_2-M_1)\cos\phi}{8}\right) - r_D\hat{I}_L^2\left(\frac{(M_2-M_1)\cos\phi}{3\pi}\right) \quad (4.17)$$

It can be inferred from (4.16) and (4.17) that if the IGBT and diode have equal threshold voltages and differential resistances, the overall change in conduction losses will be zero. Indeed, in the existing IGBT and diode power modules these parameters differ very little.

4.4. Calculation of the Minimum Required DC Bus Voltage

As explained in Section 4.2, the flexible-voltage dc-bus operation can be most effective with loads such as the prime mover (PM) of the ship, where the consumed

power is usually below the maximum level. Therefore, the dc bus voltage of the inverter driving the PM can be adjusted in proportion to the output power, which in turn depends on the load torque and speed of the PM. In this section, the method to calculate the minimum required dc bus voltage of the inverter with induction and permanent magnet synchronous motors is discussed.

4.4.1. Induction Motor

The PM is assumed to be an induction motor (IM), which is controlled employing the field orientation principle.

The stator voltage vector, $\vec{v}_s$, is defined as

$$\vec{v}_s = v_{ds} + jv_{qs} = \frac{2}{3}V_{dc}\left(s_a + s_b e^{\frac{j2\pi}{3}} + s_c e^{\frac{j4\pi}{3}}\right) \tag{4.18}$$

where v_{ds}, v_{qs} are the d–q axes stator voltages, ands_a, s_b, and s_c are switching variables that defined the states of a three-phase two-level PWM inverter [87]. For the three-phase inverter, there are eight switch states. The output voltage of the inverter is composed by these eight switching states. When the required stator voltage is determined, the optimum dc bus voltage can be calculated.

The stator voltage equations of IM in the synchronous reference frame are

$$v_{ds} = R_s i_{ds} + L_{ls}\frac{di_{ds}}{dt} + L_m\frac{d_{idm}}{dt} - \omega_e(L_{ls}i_{qs} + L_m i_{qm}) \tag{4.19}$$

$$v_{qs} = R_s i_{qs} + L_{ls}\frac{di_{qs}}{dt} + L_m\frac{d_{iqm}}{dt} + \omega_e(L_{ls}i_{ds} + L_m i_{dm}) \tag{4.20}$$

where i_{ds}, i_{qs} are the d–q axes stator currents, i_{dm}, i_{qm} the d–q axes magnetizing currents, which flow through the magnetizing inductance L_m, R_s, R_r are stator and rotor resistances,

L_{ls} is the stator leakage inductance, and ω_e is the electrical angular velocity [88]. The magnetizing currents i_{dm}, i_{qm} can be calculated as below

$$i_{dm} = i_{ds} + i_{dr} \tag{4.21}$$

$$i_{qm} = i_{qs} + i_{qr} \tag{4.22}$$

where i_{dr}, i_{qr} are the d–q axes rotor currents. Components λ_{dr} and λ_{qr} of the rotor flux vector are $\lambda_{dr} = L_r i_{dr} + L_m i_{ds}$, $\lambda_{qr} = L_r i_{qr} + L_m i_{qs}$. Taking into account that the field orientation control (FOC) is realized by aligning the reference frame on the d- axis rotor flux, the following equations can be written

$$i_{dr} = \frac{\lambda_{dr} - L_m i_{ds}}{L_r} \tag{4.23}$$

$$\lambda_{qr} = 0 \Rightarrow i_{qr} = -\frac{L_m}{L_r} i_{qs} \tag{4.24}$$

Under the steady state conditions, $i_{dr} = \frac{di_{ds}}{dt} = \frac{di_{qs}}{dt} = \frac{d_{idm}}{dt} = \frac{d_{iqm}}{dt} = 0$. Hence, in the steady state of the motor, (4.19) and (4.20) can be reduced to

$$V_{ds} = R_s I_{ds} - \omega_e \left(L_{ls} I_{qs} + L_m I_{qm}\right) = R_s I_{ds} - \omega_e K I_{qs} \tag{4.25}$$

$$V_{qs} = R_s I_{qs} + \omega_e (L_{ls} + L_m) I_{ds} = R_s I_{qs} + \omega_e L_s I_{ds} \tag{4.26}$$

where $K = L_{ls} + L_m \left(1 - \frac{L_m}{L_r}\right)$, and L_s, L_r are stator and rotor inductances, respectively. The capital letters denote the steady-state values.

As is well-known, the d-axis component of stator current in FOC controls the motor flux, while the q-axis stator current controls the motor torque:

$$\left(\frac{\lambda_{dr} - L_m i_{ds}}{T_r}\right) + \frac{d\lambda_{dr}}{dt} = 0 \tag{4.27}$$

$$T_e = \frac{3}{2} p \frac{L_m}{L_r} \lambda_{dr} i_{qs} \tag{4.28}$$

where $T_r = \frac{L_r}{R_r}$ is the rotor time constant, p is the pole-pair number, and T_e is the electromagnetic torque. Based on these considerations, the method for calculating optimum dc bus voltage is depicted in Fig. 4.4. As shown, the *d*-axis stator current is obtained from (4.27), and expressed by its Laplace transform, and the *q*-axis stator current is obtained from (4.28). The currents are then used to calculate the *d*-*q* axes stator voltage components via the steady-state inverse machine model, described by equations (4.25) and (4.26). In the final step, the minimum required dc bus voltage is calculated based on the magnitude of the stator voltage from equation (4. 18).

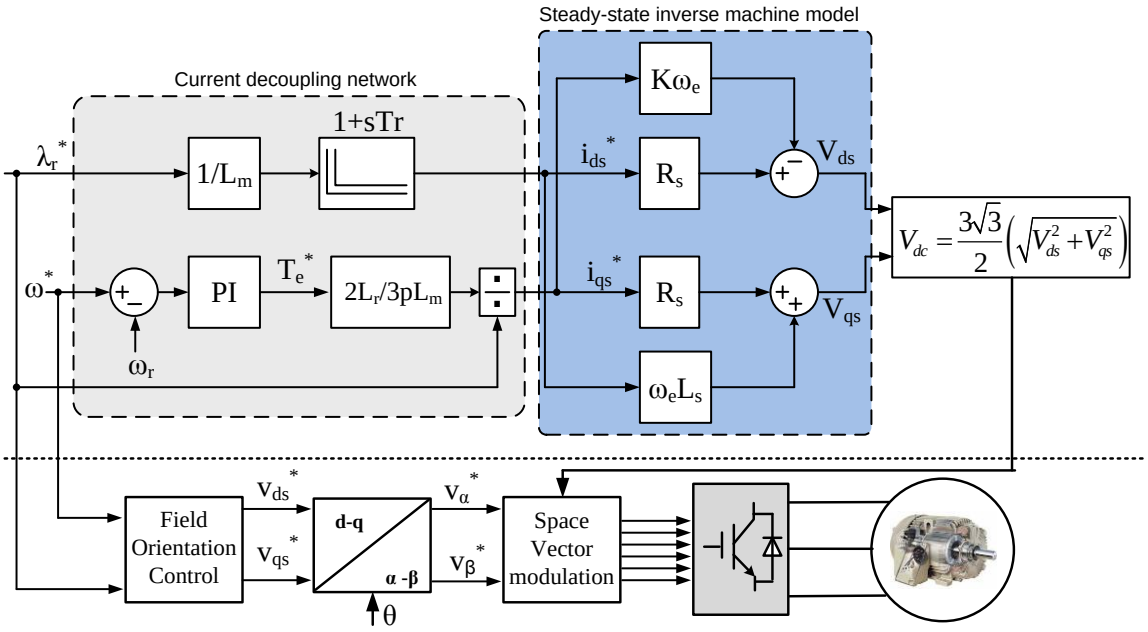

Fig. 4.4. Proposed method to calculate the minimum required dc bus voltage

4.4.2. Permanent Magnet Synchronous Motor

The fundamental component (FC) method is used in [89] to estimate *d*-axis and *q*-axis flux linkage and resulting terminal voltage. The machine speed is measured and the converter is not operated in the overmodulation region. Having this information, the

required minimum dc bus voltage is calculated. The calculation method is shown in Fig. 4.5.

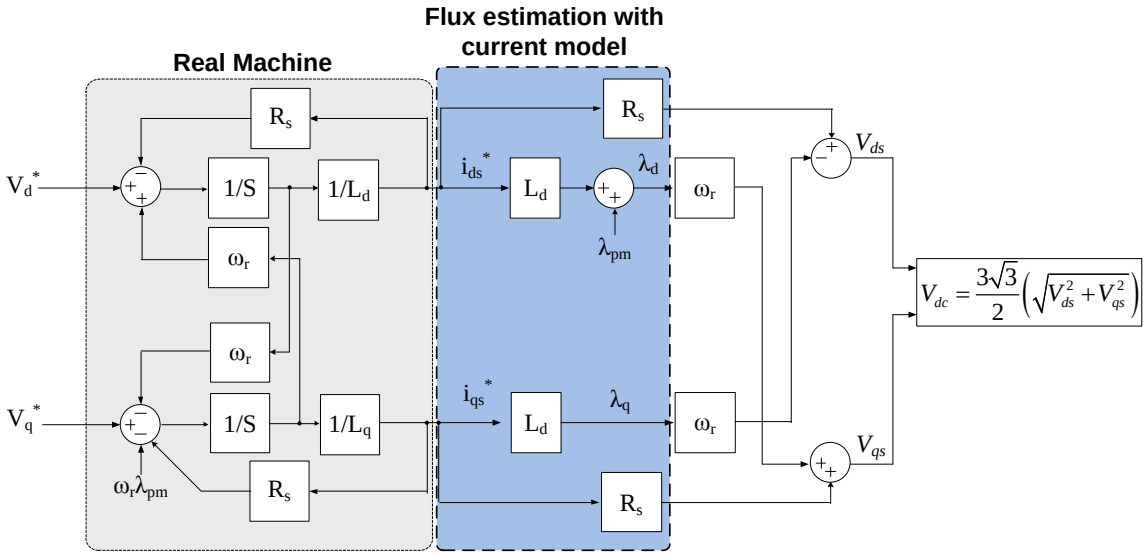

Fig. 4.5. Fundamental component method to calculate the minimum required dc bus voltage [89]

Ideally, all the motor parameters are known and remain constant during the operation of the machine. However, these parameters vary in real-time. For example, the magnetizing inductance saturates or the stator resistance changes with temperature. These uncertainties cause errors in calculating the minimum required dc bus voltage. It is experimentally verified in [89] that the required minimum dc bus voltage is much larger than what the FC model predicts. This is due to the spatial harmonics of the interior permanent-magnet synchronous machine which increase the required dc bus voltage. Therefore, a method using a voltage disturbance state filter (VDSF) is proposed in [89] to solve the calculation error problem caused by parameter variation. This method is shown in Fig. 4.6.

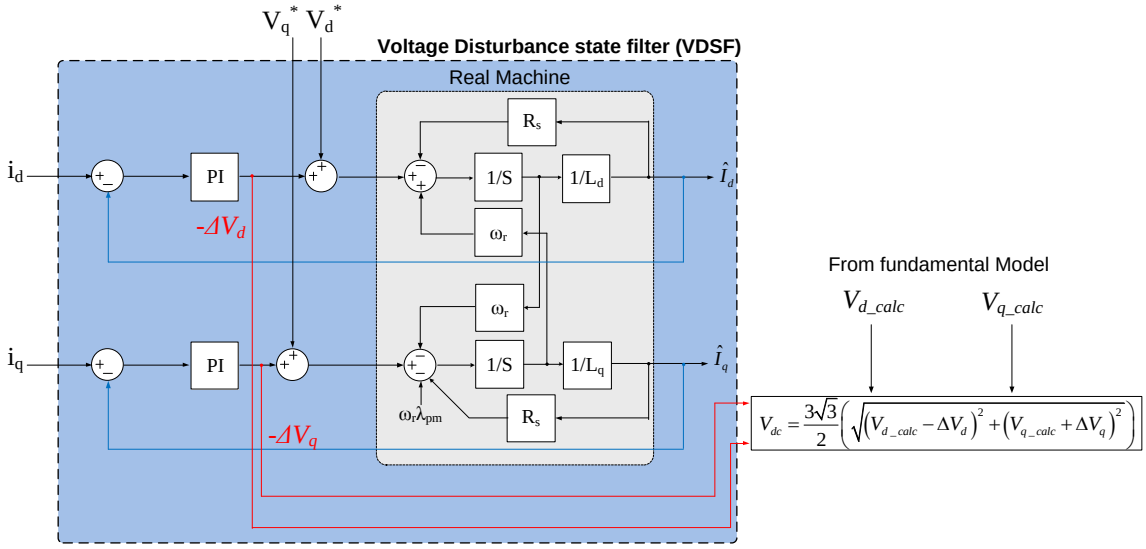

Fig. 4.6. Voltage disturbance state filter method to calculate the minimum required dc bus voltage [89]

Within its bandwidth, the stator current observer acts as a VDSF to estimate the disturbance voltage, $\Delta\hat{V}_{dq}$. This disturbance is then used to mitigate parameter uncertainties.

With correctly estimated parameters and no harmonics, the estimated current is equal to the measured current and the voltage disturbance estimate is zero. On the other hand, the voltage disturbance estimate includes the effects of parameter errors, as well as harmonics when model uncertainties are present:

$$\Delta\hat{V}_d = -\omega_r \Delta\hat{\lambda}_q = -\omega_r \Delta\hat{L}_q i_{qs} \tag{4.29}$$

$$\Delta\hat{V}_q = \omega_r \Delta\hat{\lambda}_d = \omega_r \left(\Delta\hat{L}_d i_{ds} + \Delta\hat{\lambda}_{pm}\right) \tag{4.30}$$

The voltage disturbance information is used to mitigate the parameter uncertainties which in turn are caused by saturation, temperature, and spatial harmonics.

It should be noticed that the dc bus voltage can be further reduced if the converter is operated in the nonlinear overmodualtion region. However, this can significantly increase the harmonics and result in additional losses. To overcome this drawback, several PWM

modulation techniques, such as discontinuous PWM techniques have been proposed in order to mitigate the harmonics in the nonlinear region [89]. It is also shown that the harmonics components can be as low as in the linear region. Therefore, it is still valid that selections of lowest dc bus voltage could still be the highest efficiency operating points even within the nonlinear PWM modulation region.

The theoretical lowest dc bus voltage (i.e., maximum dc bus voltage utilization) calculated using the proposed method in [89] is:

$$V_{dc} = \frac{3\sqrt{3}}{2}\sqrt{\left(V_{d\_calc} + \omega_r \Delta\hat{L}_q i_{qs}\right)^2 + \left(V_{q\_calc} + \omega_r\left(\Delta\hat{L}_d i_{ds} + \Delta\hat{\lambda}_{pm}\right)\right)^2} \qquad (4.31)$$

Chapter 5

AC-DC Power Flow

While components of microgrids and their corresponding control methodologies are fairly well understood, the system as a whole is not. When several distributed energy resources are connected to create a microgrid, the key is how to optimally manage these resources. In this chapter, the VSC's voltage-power and control equations are derived and utilized in ac-dc Newton-Raphson power flow. The power flow results confirm the generation-load balance under flexible-voltage operation.

5.1. Voltage-Power Equations of VSCs

The magnitude and frequency of a VSC's ac output voltage can be simultaneously controlled using PWM. A VSC connected to an ac bus *m* through a transformer is shown in Fig. 5.1. The coupling transformer is assumed to be ideal.

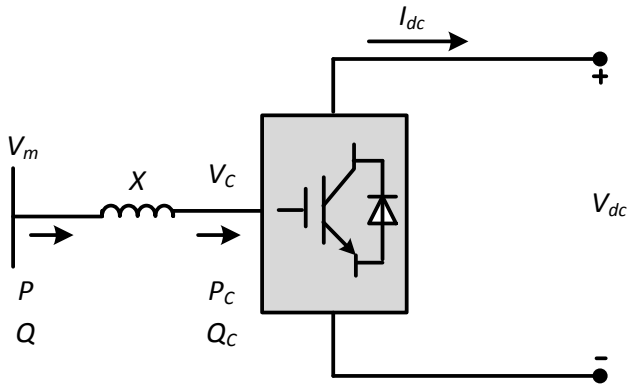

Fig. 5.1. Equivalent model of a VSC.

The converter's ac voltage, V_C, is related to the dc voltage,V_{dc}, and modulation index, *M*, as

$$V_{C_i} = \frac{M_i V_{dc_i}}{2\sqrt{2}} \tag{5.1}$$

where the subscript *i* indicates a bus number [75].

The active power across the ac bus, *P*, is calculated as

$$P_i = \frac{V_m V_{C_i} \sin(\phi_i)}{X_i} \tag{5.2}$$

where V_m denotes voltage across the m^{th} ac bus, ϕ is phase shift angle between the ac bus and converter's ac terminal voltage, and *X* is leakage reactance of the coupling transformer.

Neglecting losses in the coupling transformer, the active power flow across the VSC, P_C, is given by

$$P_{C_i} = V_{dc_i} I_{dc_i} \tag{5.3}$$

From (5.1)-(5.3), the dc current can be expressed as

$$I_{dc_i} = \frac{M_i V_m \sin(\phi_i)}{2\sqrt{2} X_i} \tag{5.4}$$

and the following equations can be used to determine the reactive power, *Q*, supplied from the ac bus *m*, and the reactive power generated by VSC, Q_C:

$$Q_i = \frac{V_m\left(V_m - V_{C_i}\cos(\phi_i)\right)}{X_i} \tag{5.5}$$

$$Q_{C_i} = -\frac{V_{C_i}\left(V_{C_i} - V_m\cos(\phi_i)\right)}{X_i} \tag{5.6}$$

The admittance matrix of the dc network, *G*, relates the dc voltages and currents of the VSCs as

$$I_{dc} = GV_{dc} \tag{5.7}$$

The phase angle, ϕ_i, between the ac bus and VSC voltages can be employed to control the flow of real power between the VSC and the network. The reactive power flow is controlled by the difference between the voltage amplitudes, $\Delta V_{C_i} = V_{m_i} - V_{C_i}$. Therefore, the real and reactive power control loops are employed to control a VSC. In the real power control loop, the VSCs are used as either power dispatchers or voltage regulators. For a system with several VSCs, one VSC is employed as a voltage regulator and the remaining VSCs are used as power dispatchers. The real power on the ac side and the voltage on the dc side are the reference values for the power dispatcher and the voltage regulator, respectively. The voltage regulator serves as a dc slack. By maintaining the dc voltage at a reference value, the voltage regulator balances the power in the dc network. Since the real power is supplied by the dc voltage regulator, it operates either as an ac-dc or a dc-ac converter. However in the reactive power control loop, either ac voltage amplitude or generated reactive power can be controlled independently for all VSCs.

If converter *i* is set to be controlled in *PQ* mode, the following equations must hold for the real and reactive powers:

$$P_{C_i} - P_{C_i}^* = 0 \qquad Q_{C_i} - Q_{C_i}^* = 0 \tag{5.8}$$

where the asterisk * denotes reference values. If converter *i* is set to be controlled under *PV* mode, the active power and ac voltage magnitude of the converter must satisfy the following conditions

$$P_{C_i} - P_{C_i}^* = 0 \qquad V_{C_i} - V_{C_i}^* = 0 \tag{5.9}$$

For a microgrid that contains several VSCs, all the converters except the dc voltage regulator are controlled in either the *PV* or *PQ* control mode.

5.2. Newton-Raphson Power Flow

To determine the power flow in autonomous microgrids, the Newton-Raphson method, with the ability to simultaneously handle both ac and dc power flows, has been applied to the voltage-power equations in Section 5.1. The dc voltage regulator is connected to the ac bus 1, which is the only slack for the entire microgrid. As already mentioned, the controllers of the remaining VSCs employ the *PQ* or *PV* mode.

In order to calculate the ac-dc power flow in the microgrid, mismatches, that are the differences between the scheduled and calculated parameters, must be determined at each bus. To calculate the reactive power mismatch at any ac bus, the following equation can be used

$$\Delta Q = Q_i^{spec} - \frac{V_m(V_m - V_{Ci}\cos(\phi_i))}{X_i} \tag{5.10}$$

The mismatch of real power between, the ac slack bus, and the dc side of the voltage regulator can be calculated as

$$\Delta S1 = \frac{V_1 V_{c_1}\sin(\phi_1)}{X_1} - V_{dc_1} I_{dc_1} \tag{5.11}$$

Here, the subscript 1 indicates the slack bus. The relation between the dc current in the slack bus and the voltages of the dc network can be expressed using the admittance matrix of the dc network. The dc current mismatch at the slack bus is given by

$$\Delta S2 = I_{dc_1} - G_1 V_{dc} \tag{5.12}$$

The remaining converters have five state variables V_{dc}, I_{dc}, V_C, M, and ϕ. Equations (5.13) and (5.14) assume that the i^{th} VSC is connected to ac bus *m*. Thus,

$$\Delta R1_i = V_{C_i} - M_i V_{dc_i} \tag{5.13}$$

$$\Delta R2_i = I_{dc_i} - \frac{M_i V_m \sin(\phi_i)}{X_i} \tag{5.14}$$

where $\Delta R1$ represents mismatch of the converter ac voltage and $\Delta R2$ represents the dc and ac networks power mismatch. The mismatch of dc current injected into dc network, $\Delta R3$, is defined as

$$\Delta R3_i = I_{dc_i} - G_i V_{dc} \tag{5.15}$$

Finally, the mismatch for the control mode equations (5.8) and (5.9) can be written as

$$\Delta R4_i = P_{C_i} - P_{C_i}^* \tag{5.16}$$

$$\begin{cases} \Delta R5_i = V_{C_i} - V_{C_i}^* & for\ PV\ control \\ \Delta R5_i = Q_{C_i} - Q_{C_i}^* & for\ PQ\ control \end{cases} \tag{5.17}$$

Equations (5.10)-(5.17) generate the Newton-Raphson power flow equations for an autonomous microgrid containing multiple VSCs, as follows [90]:

$$-\Delta E = J.\Delta X \tag{5.18}$$

$$J = -\frac{\partial \Delta E}{\Delta X} \tag{5.19.a}$$

$$X^{(k+1)} = X^{(k)} + \Delta X^{(k)} \tag{5.19.b}$$

where J is system's Jacobian matrix, and

$$X = [V \quad I_{dc_1} \quad \phi_1 \quad V_{dc} \quad I_{dc} \quad V_C \quad M \quad \phi]^T \tag{5.20.a}$$

$$\Delta E = [\Delta Q \quad \Delta S1 \quad \Delta S2 \quad \Delta R1 \quad \Delta R2 \quad \Delta R3 \quad \Delta R4 \quad \Delta R5]^T \tag{5.20.b}$$

$$\Delta X = [\Delta V \quad \Delta I_{dc_1} \quad \Delta \phi_1 \quad \Delta V_{dc} \quad \Delta I_{dc} \quad \Delta V_C \quad \Delta M \quad \Delta \phi]^T \tag{5.20.c}$$

Power flow equations (5.18)-(5.19) must be solved iteratively until the termination criterion is satisfied. The termination criterion occurs when the maximum mismatch is lower than a specified threshold value, ϵ,, e.g., 0.0001. Once the termination criterion is satisfied, X yields the result of the ac-dc power flow with the desired accuracy and determines the state of the power system.

Chapter 6

Optimal power Flow

In autonomous microgrids that are studied in this dissertation, the optimal dc voltage reference for the one VSC that operates in the voltage regulator mode, and the optimal reference power settings of the remaining VSCs in the power dispatcher mode have to be pre-determined. Emulating the utility grid, these settings and control modes are commonly selected such that the dc voltage is maintained within desired margins, typically ±5 % around the rated value. In this dissertation, that problem is formulated as an optimization problem with the objective function of minimizing the converter losses. All the operational modes and limits of VSCs have been taken into account. Genetic algorithm, which is a computational intelligence technique, has been utilized in solving the optimization problem. This method is proposed as another approach to voltage and power control of VSCs in order to reduce losses.

In the following sections, a review of following optimization methods is presented: (1) Linear Programming method, (2) Newton- Raphson method, (3) Quadratic Programming method, (4) Nonlinear Programming method, and (5) Artificial Intelligence methods.

6.1. Linear Programming Method

Linear programming (LP) formulation requires the linearization of the objective function as well as linear constraints [91].

Chung *et al.* [92] minimized line losses and found the optimal capacitor allocation in distribution systems by using a recursive linear programming based approach. The proposed method is tested on IEEE 14-bus system. It does not require matrix inversion which reduces computational time and requires less memory space.

An effort is carried out in [93] for minimization of transmission losses and Generator reactive margins of the Spanish power system using LP based optimal power flow (OPF). Integer variables are used to model the discrete nature of shunt reactors and capacitors. Both the objective function and the constraints are linearized in each iteration and therefore, this method is superior to methods that linearize the objective function only.

Lima *et al.* [94] used Mixed Integer Linear Programming for optimal placement of Thyristor Controlled Phase Shifter Transformers (TCPSTs) in large-scale power systems. The objective is to find the number, network location and settings of TCPSTs that maximize system loadability. The constraints are the installation investment and limited number of TCPSTs. The proposed method requires much less computational time compared to other published cases.

6.2. Newton-Raphson method

The necessary conditions of optimality, referred to as the Kuhn-Tucker conditions, are obtained in this method [91].

S.Chen *et al.* [95] employed a Newton-Raphson (NR)-based algorithm to solve emission dispatch problem. The developed Jacobian matrix and the B-coefficients depend on the generalized generation shift distribution factor. The proposed method requires less computational time compared to the conventional Newton-Raphson method.

Two versions of NR method were proposed in [96]: the Fixed Newton method and the modification of the right-hand-side vector method. The case studies have verified that the proposed methods have better convergence characteristics compared to the Newton-based load flow method.

Semi-smooth Newton-type algorithm was proposed in [97] for solving OPF problems. In this method, inequality constraints and bounded constraints are handled separately. A diagonal matrix and the nonlinear complementarity function are employed to transform the OPF system to an equivalent system of non-smooth bounded constrained equations. This method requires less computational time due to less number of variables.

6.3. Quadratic Programming Method

Quadratic programming is a special form of nonlinear programming with quadratic objective function and linear constraints [91].

OPF was formulated as a generalized Quadratic-Based problem in [98]. The conditions for feasibility, convergence and optimality are included in the optimization problem. The proposed method is capable of optimizing multiple objective functions with selectable constraints. The proposed method features reduced memory use and execution time.

Lin *et al.* [99] used sequential quadratic programming to optimally solve the integrated cost and voltage stability analysis for competitive markets. IEEE 14-bus test system is employed to obtain optimal reactive power dispatch under various voltage stability margin requirements under normal and faulty grid conditions.

The optimal setting and operation mode of UPFC and TCPAR were determined in [100] using Security–Constrained Optimal Power Flow (SCOPF). Han-Powell method is

used to solve the optimization problem. This method employs solution of successive quadratic problems with linear constraints to solve nonlinear problems with nonlinear constraints.

6.4. Nonlinear Programming Method

Nonlinear programming (NLP) is employed to solve problems with nonlinear objective functions and/or constraints [91].

Reference [101] presented a nonlinear convex network flow programming (NLCNFP) model and algorithm for solving the security-constrained multi-area economic dispatch (MAED) problem. The tie-line security and transfer constraints in each area are considered in the MAED model. A simple analysis of a buying and selling contract in a multi-area environment is also made. The test results on four interconnected power systems confirm the feasibility and effectiveness of the proposed method.

LP and NLP based reactive OPF were employed in [102] for auctioning reactive power among competing utilities in a deregulated power system. LP method calculated the overall cost associated with the system reactive power requirement reasonably accurately, but convergence of NLP could not be guaranteed for every operating condition. On the other hand, NLP features less computational time and higher accuracy.

The cost of reactive power support service in a multi-area power system was formulated as an optimization problem and solved in [103] using cost-benefit analysis (CBA) and nonlinear convex network flow programming. The proposed methods compute the reactive power support benefits with respect to increases in the delivered power in distribution lines.

Reference [104] proposed a method of optimal number and location of TCSC using mixed integer nonlinear Programming approach in the deregulated electricity markets. The system loadability has been determined in a hybrid market model utilizing the secure transaction matrix. The proposed technique was tested on IEEE 24-bus test system.

6.5. Artificial Intelligence Methods

Due to the approximations introduced with the linearized models, the aforementioned conventional methods may not give the optimal solution for inherently non-linear, non-differentiable objective functions. These conventional methods are also known to converge to a local optimal rather than the global solution.

6.5.1. Artificial Neural Network Method

Chowdhury *et al.* [105] introduced key ideas behind the concept of an integrated security constrained optimal dispatch (ISCOD). Its purpose is to calculate the optimal power outputs of generators and the voltage magnitude of buses so that the cost of power generation is minimized while both static and dynamic security of the system are maintained. ISCOD combines the diagnostic and decision making capabilities of Knowledge Base System (KBS) and the massive parallelisms and learning features of an artificial neural network (ANN) along with conventional power system network solution methodologies to provide real-time control and optimization.

A two-stage ANN was proposed in [106] to control the multi tap capacitors installed on a distribution system for a nonconforming load profile. The purpose is to minimize the system losses. The active and reactive powers, voltage magnitudes and the current capacitor settings at certain buses are measured and used as input data. Inequality constraints consist of limits on capacitor ratings. The computation time required for the

learning process limits the application of the proposed method. The computation time is high because it depends on the number of conforming load groups and capacitors installed rather than the number of system buses.

6.5.2. Fuzzy Logic Method

A fuzzy model for power system operation was presented in [107]. Uncertainties in loads and generations are modeled as fuzzy numbers. System behavior under known, while uncertain, injections is dealt with DC fuzzy power flow model. System optimal operation is calculated with LP procedures where the problem nature and structure allows some efficient techniques such as Dantzing Wolfe decomposition and dual simplex to be used. Among the results, a fuzzy cost value for system operation and possibility distributions for branch power flows and power generations are obtained.

Reference [108] presented a fuzzy logic approach for the contingency constrained OPF problem formulated in a decomposed form that allows for post-contingency corrective rescheduling. The formulation treats the minimization of both the base case (pre-contingency) operating cost and of the post-contingency correction times as conflicting but fuzzy goals. The main contribution of the paper is the development of a systematic procedure for specifying the tolerance parameters that are needed to obtain fuzzy membership functions for these fuzzy goals. The fuzzy formulation is then converted into a crisp formulation that is solved using a standard OPF method.

An efficient and practical hybrid model for congestion management analysis for both real and reactive power transaction under deregulated fuzzy environment of power system was proposed in [109]. The proposed model determines the optimal bilateral or multilateral transaction and their corresponding load curtailment in two stages. In the first

stage, classical gradient descent OPF algorithm was used to determine the set of feasible curtailment strategies for different amount of real and reactive power transactions, whereas in the second stage, a fuzzy decision opinion matrix was used to select the optimal transaction strategy considering increase in private power transaction, reduction in percentage curtailment, and its corresponding change in per unit generation cost and hence profit as fuzzy variables.

6.5.3. Ant Colony Optimization

Yu *et al.* [110] presented a novel co-operative agents approach, Ant Colony Search Algorithm (ACSA)-based scheme, for solving a short-term generation scheduling problem of thermal power systems. The main purpose of the paper is to investigate the applicability of an alternative intelligent method in power system optimization, particularly in short-term generation scheduling problems. The ACSA is derived from the theoretical biology of the topic of ant trial formation and foraging methods. A set of co-operating agents, ants, co-operate to find a good solution for the short-term generation scheduling problem of thermal units. The effectiveness of the proposed scheme has been demonstrated on the daily generation scheduling problem of model power systems.

In [111], an ant colony optimization algorithm with random perturbation behavior (RPACO) based on combination of general ant colony optimization and stochastic mechanism was developed for the solution of optimal unit commitment (UC) with probabilistic spinning reserve determination. The security function approach is applied to evaluate the desired level of system security. PRACO is adopted to solve the UC problems. Furthermore, the sensitivity of the desired security level to the optima during optimization is investigated.

A procedure to determine the maximum reliability of series-parallel electrical power system topology was proposed in [112]. In this procedure, electrical system devices are characterized by their reliability, performance and cost. To evaluate the system reliability, a universal moment generating function (UMGF) approach is used by the ant colony algorithm to determine the optimal electrical power network topology.

6.5.4. Particle Swarm Optimization

This approach is based on the ideas of social behavior of organisms such as animal flocking and fish schooling.

Reference [113] proposed a Particle Swarm Optimization (PSO) for reactive power and Voltage/VAR Control (VVC) considering voltage security assessment. The proposed method expands the original PSO to handle a mixed-integer nonlinear optimization problem and determines an on-line VVC strategy with continuous and discrete control variables such as automatic voltage regulator operating values of generators, tap positions of on-load tap changer of transformers, and the number of reactive power compensation equipment.

A Modified Particle Swarm Optimization (MPSO) mechanism was proposed in [114] to deal with the equality and inequality constraints in the economic dispatch problems. Moreover, a dynamic search-space reduction strategy is devised to accelerate the optimization process. The results obtained from the proposed method are compared with those obtained by aforementioned methods and shown to yield superior results.

A Modified Particle Swarm Optimization (MPSO) was presented in [115]. In this algorithm, particles not only studies from itself and the best one, but also from other

individuals. By this enhancement, the opportunity to find the global optimum is increased and the influence of the initial position of the particles is decreased.

In [116], the contributions of generators to the power flows in transmission lines were formulated as a multi-objective optimization problem and calculated using a Parallel Vector Evaluated Particle Swarm Optimization (VEPSO) algorithm. Specifically, the generator contributions to the transmission system are modeled by particles of swarms whose positions are optimally determined while satisfying all multi-objectives and other physical and operating constraints. The proposed VEPSO algorithm accounts for nonlinear characteristics of the generators and transmission lines. The experimental results show that the proposed method is capable of obtaining precise solutions compared to analytical methods while considering nonlinear characteristics of the system.

Reference [117] presented the application of Particle Swarm Optimization technique to find the optimal location of FACTS devices with minimum cost of installation of FACTS devices and to improve system loadability. While finding the optimal location, the thermal limit for the lines and voltage limit for the buses are taken as constraints. Three types of FACTS devices, thyristor controlled series compensator (TCSC), static VAR compensator (SVC) and unified power flow controller (UPFC) were considered.

6.5.5. Genetic Algorithm Method

Chen *et al.* [118] presented a genetic approach for solving the economic dispatch problem in large-scale systems. A new encoding method is developed. The chromosome contains only an encoding of the normalized system incremental cost in this encoding technique. Therefore, the total number of bits of chromosome is entirely independent of the number of units. This makes the proposed genetic approach attractive in large and

complex systems which other methodologies may fail to achieve. Moreover, the approach can take network losses, ramp rate limits and prohibited zone avoidance into account because of genetic algorithm's flexibility.

A Hybrid GA method was presented in [119] to solve OPF in power systems including FACTS devices. GA-based OPF is employed for minimizing total generation fuel cost, while satisfying the security limits. A case study using IEEE 14-bus test system is presented to demonstrate the proposed methods applicability.

The optimal choice and allocation of FACTS devices in multi-machine power systems using genetic algorithm was presented in [120]. The objective is to achieve the power system economic generation allocation and dispatch in deregulated electricity market. Using the proposed method, the locations of the FACTS devices, their types and ratings are optimized simultaneously. Different kinds of FACTS devices and their investment costs are considered.

6.6. Problem Formulation

OPF is formulated mathematically as a general constrained optimization problem:

$$\begin{aligned} &Min\ F(u,x) \\ Subject\ to \quad &h(u,x) = 0 \\ and \quad &g(u,x) \geq 0 \end{aligned} \tag{6.1}$$

Here, u is the set of controllable quantities in the system and x is the set of dependent variables. $F(u,x)$ is a scalar objective function. Equality constraints are derived from conventional power balance equation. Inequality constraints are the limits on control variables u and the operating limit on the other variables of the system [91].

6.6.1. Objective Function

The objective is to find voltage and power settings which minimize the power electronics converter losses. Switching and conduction losses are modeled for three-phase, two-level VSCs with six IGBT and six diode switching devices.

Equation (4.9) was used to calculate the switching losses of a VSC with sinusoidal ac line current and IGBT switches. That equation is repeated here for the sake of convenience:

$$P_{sw} = \frac{6}{\pi}.f_{sw}.\left(E_{ON,I} + E_{OFF,I} + E_{OFF,D}\right).\frac{V_{dc}}{V_{ref}}.\frac{\hat{I}_L}{i_{ref}} \tag{6.2}$$

Furthermore, the diode and IGBT conduction losses were calculated using equations (4.13)-(4.14), as follows:

$$P_{C,IGBT} = u_{ce0}\hat{I}_L\left(\frac{1}{2\pi} + \frac{M\cos\alpha}{8}\right) + r_c\hat{I}_L^2\left(\frac{1}{8} + \frac{M\cos\alpha}{3\pi}\right) \tag{6.3}$$

$$P_{C,Diode} = u_{D0}\hat{I}_L\left(\frac{1}{2\pi} - \frac{M\cos\alpha}{8}\right) + r_D\hat{I}_L^2\left(\frac{1}{8} - \frac{M\cos\alpha}{3\pi}\right) \tag{6.4}$$

The converter losses can be formulated using equations (6.2)-(6.4) as:

$$P_{loss} = P_{sw} + 6\left(P_{C,IGBT} + P_{C,Diode}\right) \tag{6.5}$$

Finally, the objective function can be written as

$$F = \sum_h (P_{loss})_h \tag{6.6}$$

where *h* denotes the total number of VSCs in the microgrid.

6.6.2. Equality Constraints

The equality constraints are basically the mismatch equations (5.10)-(5.17). As the power flow converges to the final solution, the mismatches converge to zero.

6.6.3. Inequality Constraints

The ac generators can produce a limited amount of real and reactive power. Therefore, the following constraints must be applied at generator buses:

$$P_{G,min} \leq P_{G_i} \leq P_{G,max} \tag{6.7}$$

$$Q_{G,min} \leq Q_{G_i} \leq Q_{G,max} \tag{6.8}$$

Here, subscript *i* indicates the generator bus number.

The voltages of ac buses should remain in a specific range in order to ensure the quality of the voltage:

$$V_{m,min} \leq V_{m_j} \leq V_{m,max} \tag{6.9}$$

where subscript *j* denotes ac bus number. Typically, the ac voltage limits are $0.95 \leq V_m \leq 1.05$ p.u. Furthermore, the power of VSC should not exceed its rated value:

$$P_{C_j} \leq P_{C,rated} \tag{6.10}$$

In the microgrid under study, a dc distribution network is utilized. The power flowing from dc bus *k* to dc bus *l* through a cable with resistance of R_{dc}, can be calculated as follows:

$$P_{Line} = V_{dc_k}\left(\frac{V_{dc_k} - V_{dc_l}}{R_{dc}}\right) \tag{6.11}$$

For secure operation, the power through the distribution line should not exceed its flow limits:

$$P_{Line} \leq P_{max} \tag{6.12}$$

In the existing studies, the dc bus voltages are fixed to the rated value or kept in a narrow band. Here, however, the dc bus voltages of VSCs, including the voltage

regulator, are allowed to fluctuate in a wide range, and their only limit is the rated value, that is:

$$V_{dc_j} \leq V_{dc,rated} \tag{6.13}$$

The reason for such a control strategy lies in the discussion presented in Chapter 4. Since, for a given fundamental voltage low and wide voltage pulses result in lower switching losses than high and narrow ones, it would be more efficient to employ the minimum possible dc bus voltage and a high modulation index rather than constantly maintain a high dc bus voltage. It must be pointed out that reduction of the dc bus voltage may not result in over-modulation, i.e.,

$$0 \leq M_j \leq 1 \tag{6.14}$$

Fig. 6.1 shows the GA-based OPF algorithm, whose steps are:

1. An initial population is randomly generated within the search space.
2. The fitness of each individual is assessed using the fitness (objective) function.
3. The solution that is more likely to survive in the next generation is chosen by the selection operator.
4. Using crossover and mutation operators, the new population is generated.
5. The fitness of the new population is assessed.
6. If both the equality and inequality constraints are satisfied, the algorithm is terminated. Otherwise, a return is made to the third step.
7. After termination, the algorithm returns the optimal solution, which is the global solution to the problem.

A detailed description of crossover, mutation, fitness evaluation, and selection operators are given below:

A. *Crossover:* This operator is used to produce new population using the features of the existing ones. After selecting parents from the population, the crossover points are selected. The crossover points are selected randomly, such that the distribution from which the points are drawn is uniform. One-point and two-point crossovers are among the most common techniques reported in the literature. Once the points are defined, two offspring items are generated by interchanging the values between the two parents. In GA, crossover is the operator that spreads the favorable characteristics of the members around the population.

B. *Mutation:* This operator produces new characteristics in the members of the population. A mutation operator is vital in exploring the promising areas and preventing the population from converging to local optima. Mutation operator assists the algorithm in converging to the global optimum.

C. *Fitness evaluation:* After manipulating the population using the crossover and mutation operators, the fitness of each new offspring is evaluated through the fitness (objective) function.

D. *Selection:* Within this operation, it is determined which parents should take part in producing offspring for the next generation. There is an analogy between this operation and “survival of the fittest” in nature, where the weakest individuals in the population are eliminated.

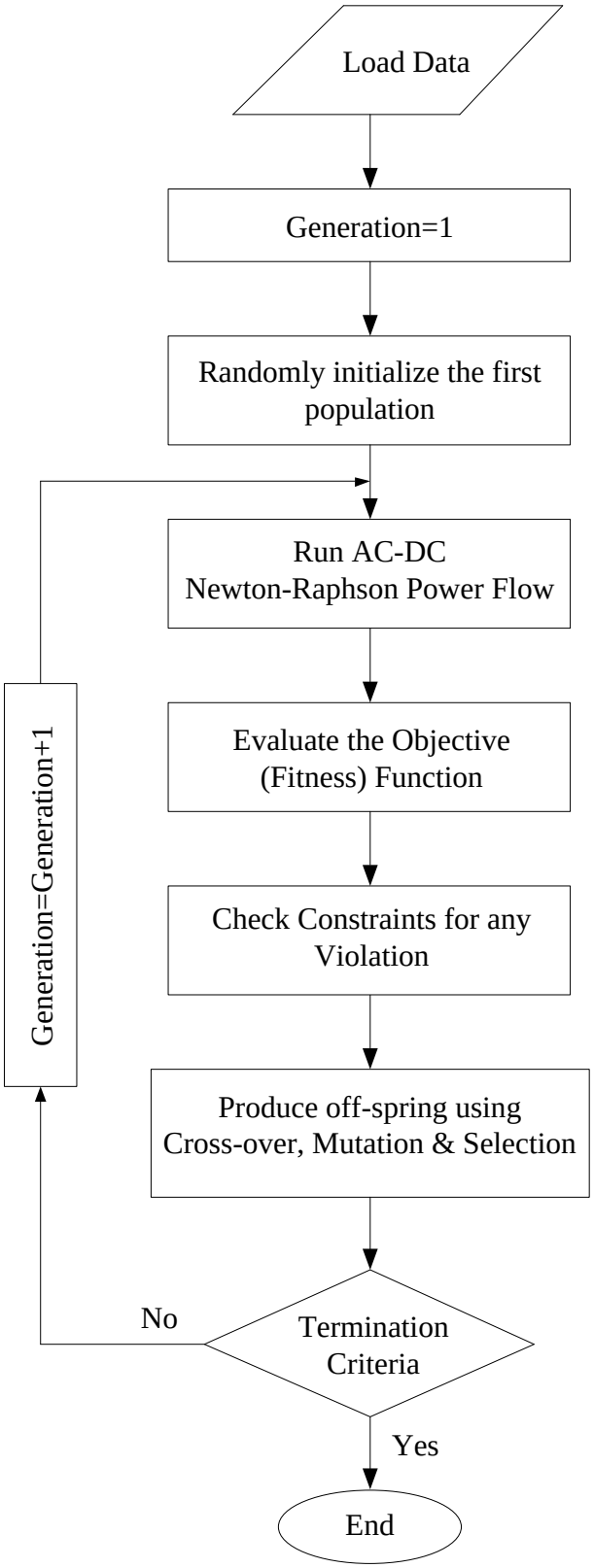

Fig. 6.1. GA-based OPF flowchart.

Chapter 7

Case Studies

The power flow in a microgrid was investigated using the simplified model of MVDC SPS shown in Fig. 7.1. The model consists of ten ac buses connected to ten dc buses using VSCs. The dc buses are connected through twelve dc cables. The coupling transformer reactance and dc cables resistance are 0.1p.u. and 0.03 p.u., respectively. Bus 1 is the slack bus and, consequently, the VSC connected to it acts as the only voltage regulator. The generators are connected to buses 1, 3, 4 and 6, and the propulsion induction motor is fed from bus7. Buses 2, 5 and 8 through 10 feed five zonal loads. The VSCs that interface the generators with dc buses 3, 4, and 6 act as rectifiers and those who supply the loads from dc buses 2, 5, 7, 8, 9, and 10 act as inverters. All the VSCs are controlled in the *PV* mode. The generation and load values are shown directly in the figure.

The induction motor's daily load profile in Fig. 7.2 shows the hourly active power consumption of the motor. The peak power value is 1.6 MW, and it is assumed that the ship slows down in the night and cruises during the daytime. The generators at buses 3, 4 and 6 constantly supply 9 MW, and the slack generator picks up the slack.

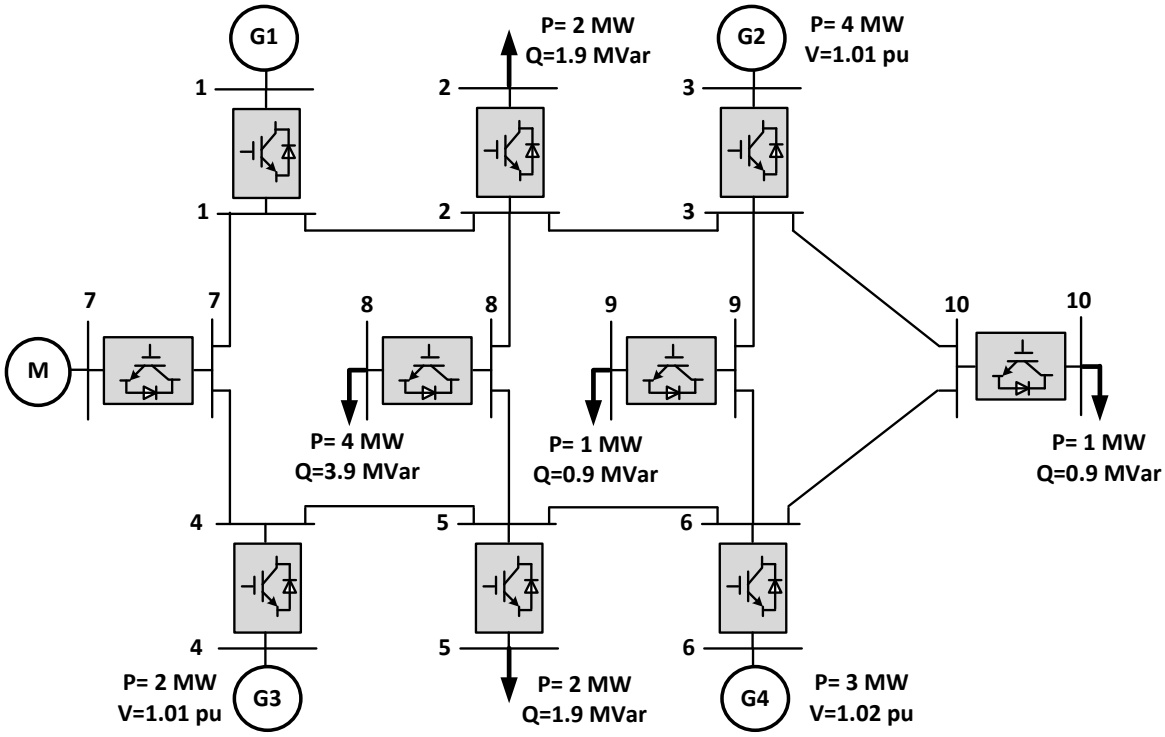

Fig. 7.1. Simplified model of the MVDC SPS.

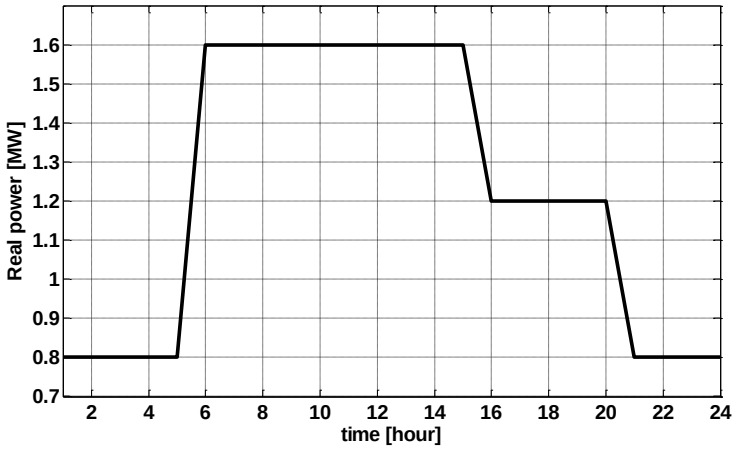

Fig.7.2. Daily motor load profile

7.1. Power Flow Results

To illustrate the flexible-voltage idea, MATLAB was used and the power flow was determined for the model MVDC SPS using Eqs. (5.10)-(5.19) for two cases. In the first

case, the voltage regulator VSC connected to the slack bus was set to generate a dc voltage of 1.05p.u.during the entire day. In the second case, the reference output of the voltage regulator was adjusted such that the calculated minimum dc bus voltage for the induction motor drive was obtained on dc bus 7. This was carried out in two steps:

1. A 1.6 MW induction motor with the parameters listed in Table II was fed through a three phase inverter. In order to obtain the same motor load profile as in Fig. 7.2, the load torque was set to 16×10^3 Nm and the reference speed was varied as in Fig. 7.3. The minimum required dc voltage value was calculated using the method proposed in chapter four and was used as the input to a look-up table.
2. The look-up table provides the corresponding dc reference value for the voltage regulator at bus 1. The data for the look-up table has been produced by running the power flow in the power system in Fig. 7.1 with the same generated and load powers, but with V_{dc_1} varied from 0.9 to 1.05 p.u. in steps of 0.001 p.u. and saving the corresponding V_{dc_7} values. Thus, for each dc voltage value at bus 7 a reference value would be available for the voltage regulator at bus 1.

The selected ac bus data for both cases are presented in Figs. 7.4 and 7.5, and the converter variables are shown in Figs. 7.6-7.8.

Table II. PARAMETERS OF THE SIMULATED INDUCTION MOTOR

f	P	R_r	R_s
60 Hz	1.6 MW	0.0455 Ω	0.0407 Ω
$L_s = L_r$	L_m	**Pole Pairs**	**J**
0.02702 H	0.02595 H	3	10 kg.m^2

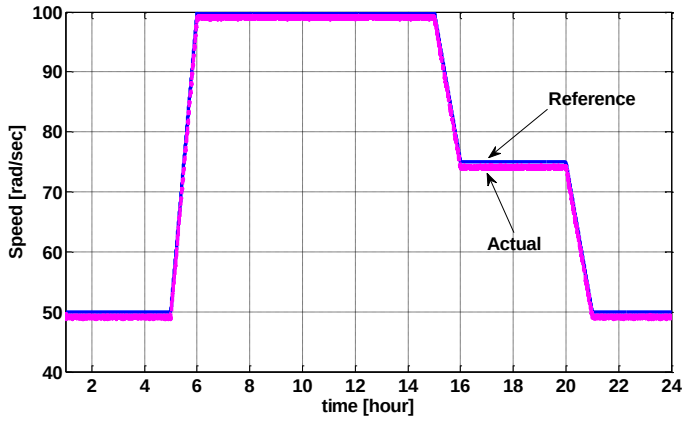

Fig. 7.3. The reference and actual speeds.

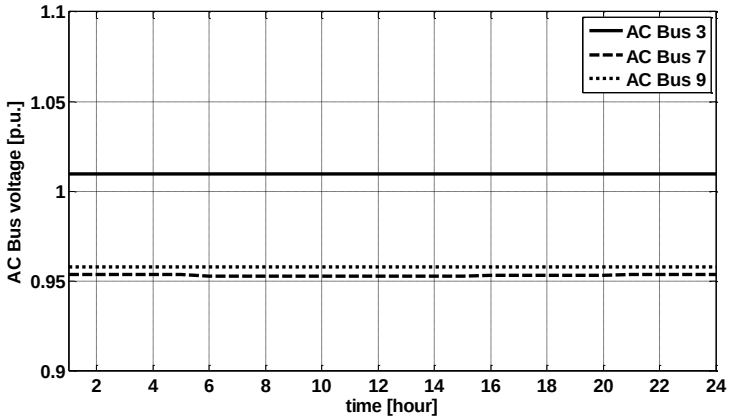

(a)

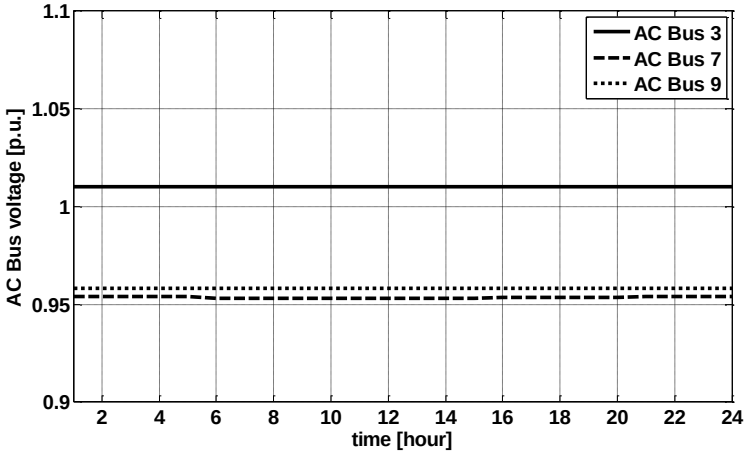

(b)

Fig. 7.4. Selected ac bus voltages in the model MVDC system: (a) Case I, (b) Case II.

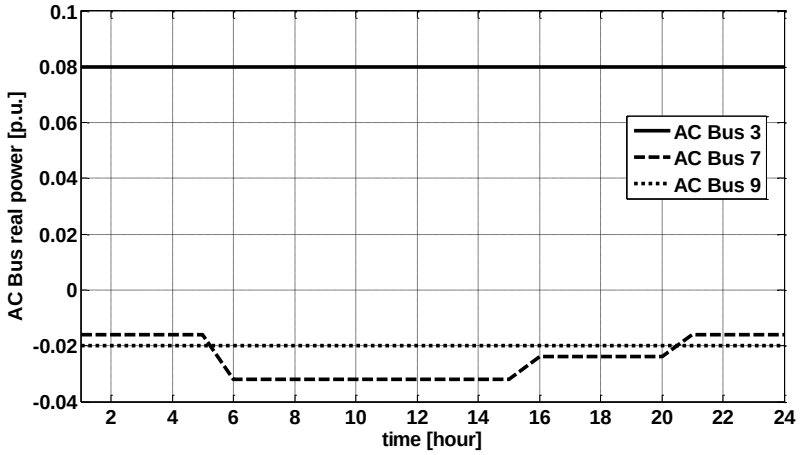

(a)

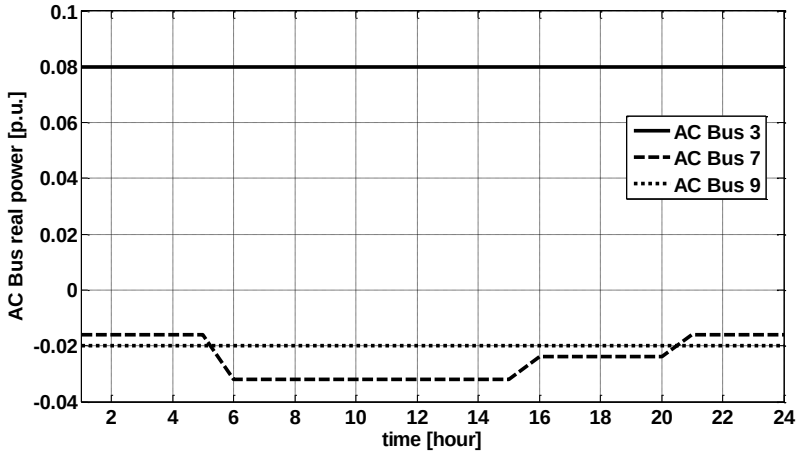

(b)

Fig. 7.5. Selected ac bus real powers in the model MVDC system: (a) Case I, (b) Case II.

It is seen from Figs.7.4 (a) and (b) that the ac bus voltages remain in the 0.95-1.05 p.u. range for the both cases. Figs. 7.5 (a) and (b) depict the real power supplied by the generator at bus 3, and the consumed load at bus 9 and 7. It should be noted that the base apparent power was selected as 50 MVA. As shown, the demand at buses 9 and 7 is fully satisfied during the 24-hour period using the proposed method. Also, the results imply that

there is a balance between the generation and load at each bus which makes the MVDC SPS stable during the 24-hour period and causes the power flow to converge.

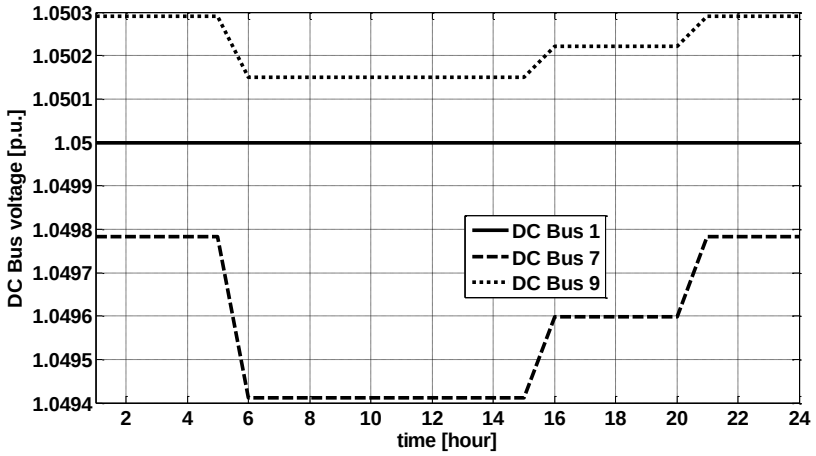

(a)

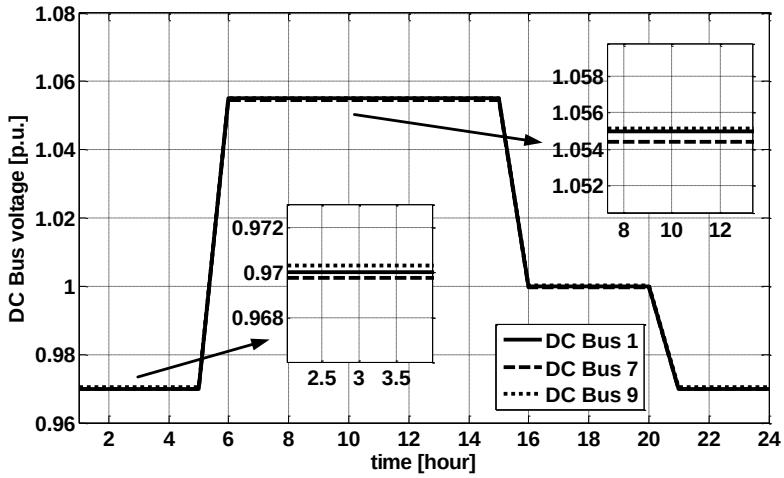

(b)

Fig. 7.6. Selected dc bus voltages in the model MVDC system: (a) Case I, (b) Case II.

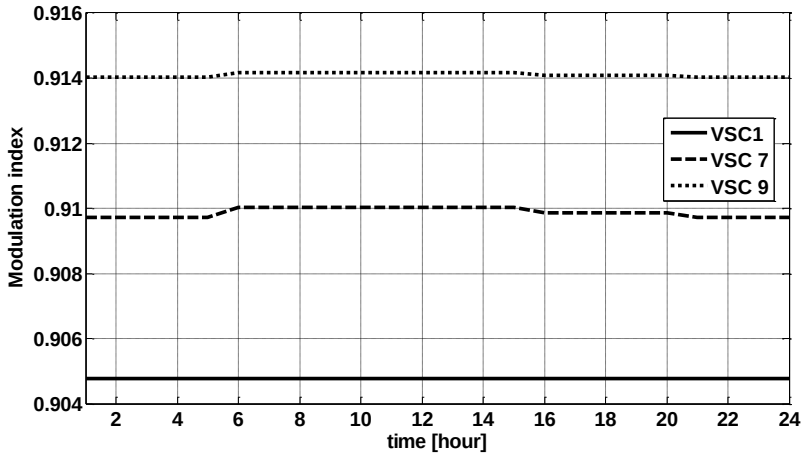

(a)

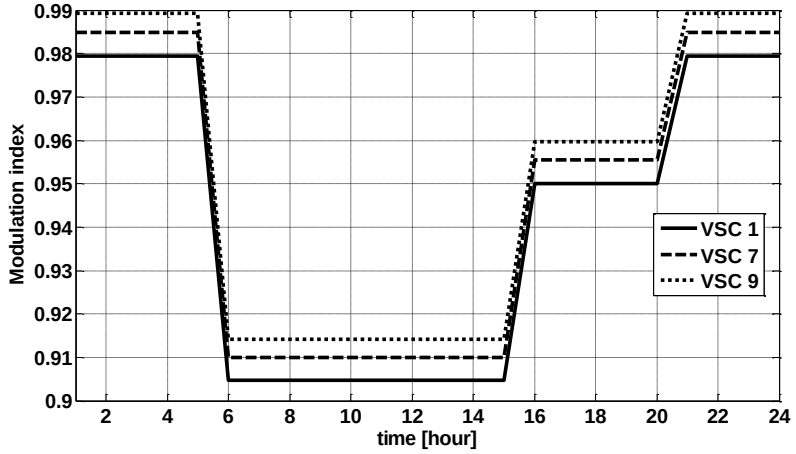

(b)

Fig. 7.7. Selected modulation indices in the model MVDC system: (a) Case I, (b) Case II.

Fig. 7.6 depicts the dc bus voltage in the MVDC SPS for the both cases. As seen, in the second case the dc regulator sets the dc link voltage to a lower level during off-peak load hours. At full loads, the dc link voltage is increased to the rated value. The modulation indices of selected converters are shown in Fig. 7.7. When the dc link voltage is reduced, the corresponding modulation index increases to maintain the required voltage at the output of the converter. In this way, to deliver a given amount of power to the

loads, the current drawn from the generators remains the same. This can be verified by examining Figs. 7.8 (a) and (b), which depict the dc distribution currents.

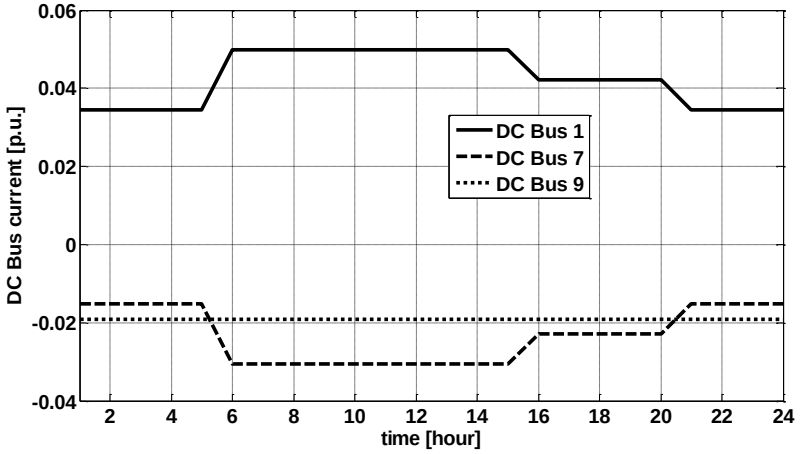

(a)

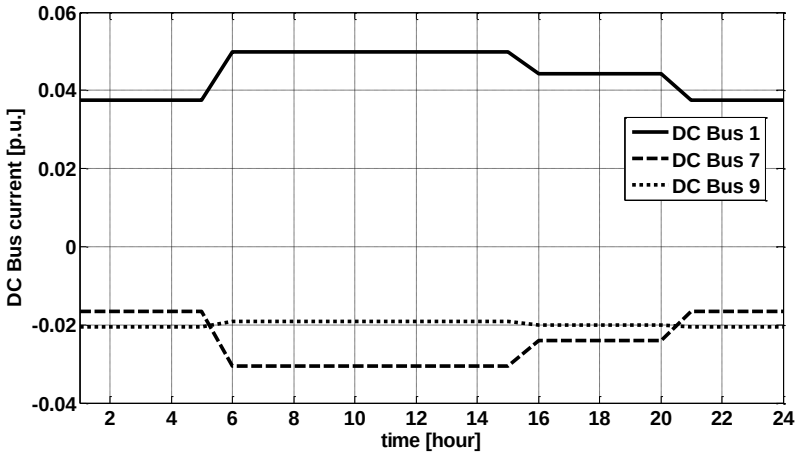

(b)

Fig. 7.8. Selected dc bus currents in the model MVDC system: (a) Case I, (b) Case II.

7.2. Switching and Conduction Losses

To verify the effectiveness of the flexible-voltage dc-bus operation in reduction of the switching losses, two cases of different dc link voltages and modulation indices but of the same load torque and speed were modeled. The dc link voltages and modulation indices

were obtained from the ac-dc power flow results. In the first case, the dc source and modulation index values from Figs. 7.7(a) and 7.8(a) were employed to supply the inverter. In order to obtain the same motor load profile as shown in Fig. 7.2, the load torque was set to 16×10^3Nm and the reference speed was varied as in Fig. 7.3. In the second case, the same scenario, but with decreased source voltage and increased modulation indices from Figs. 7.7(b) and 7.8(b) was played out.

The IGBT and diode parameters were obtained from the datasheet of a 3300 V, 1500 A power module (FZ1500R33HE3), and are listed in Table III. The parameters of a GTO thyristor were obtained from [83] and are given in Table IV. The simulation results are shown in Figs. 7.9 and 7.10. The reduced supply voltage results in reduced switching losses, while the conduction losses are practically the same. Since the motor operates with the same output power, reduction in the switching losses represents an increased efficiency.

Table III. Parameters of the simulated IGBT and diode

$E_{ON,I}$	V_{ref}	u_{D0}
2550 mJ	1800 V	1.75 V
$E_{OFF,I}$	I_{ref}	r_C
2100 mJ	1500 A	0.001 Ω
$E_{OFF,D}$	u_{ce0}	r_D
1650 mJ	1.6 V	0.00067 Ω

Table IV. Parameters of the simulated GTO

E_g	V_B	τ_a
1.11 eV	5000 V	2 μs
E_C	kT/q	L_a
0.3×10^6 V/cm	0.026 V	29.4 μm
ε	μ_n	q
11.8	65 cm^2/V.s	1.6×10^{-19} C

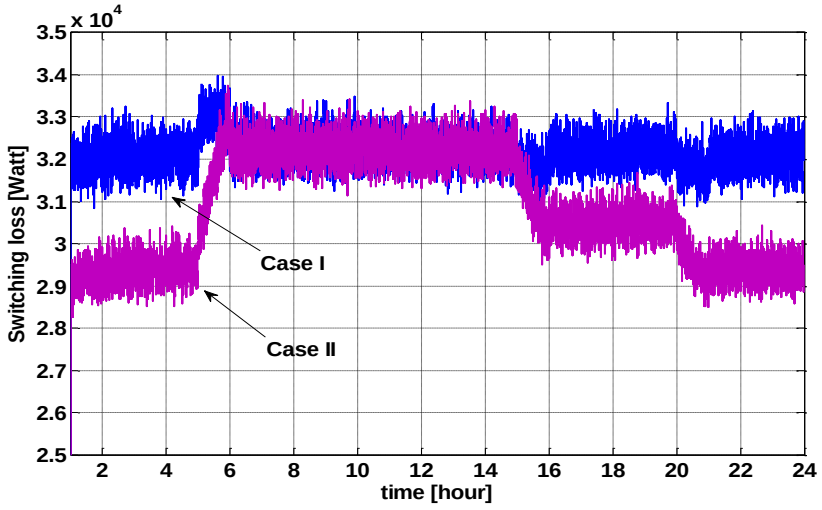

(a)

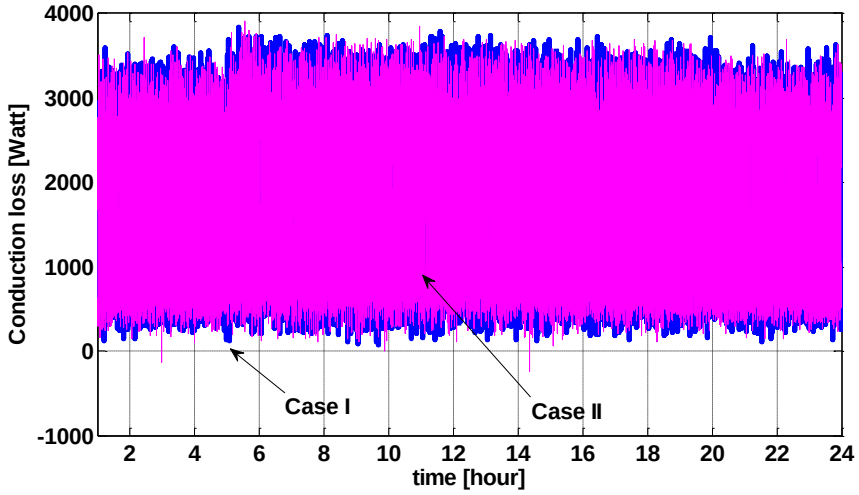

(b)

Fig. 7.9. IGBT-based VSC, (a) Switching losses in cases I & II, (b) Conduction losses in cases I & II.

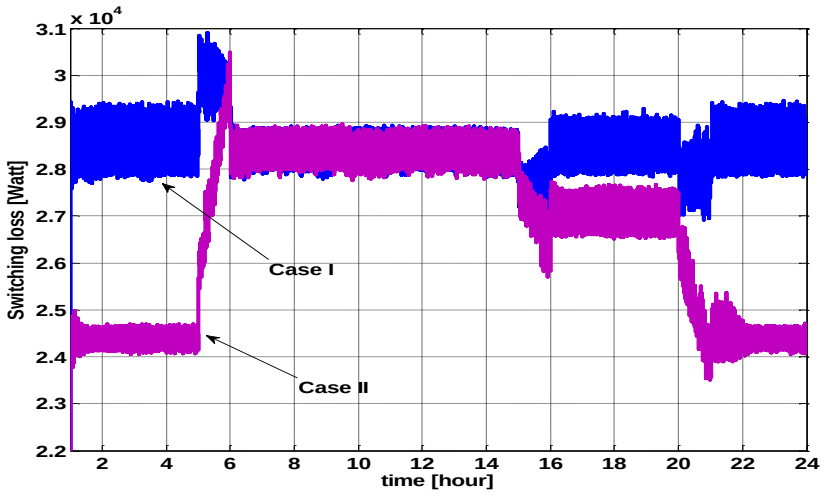

(a)

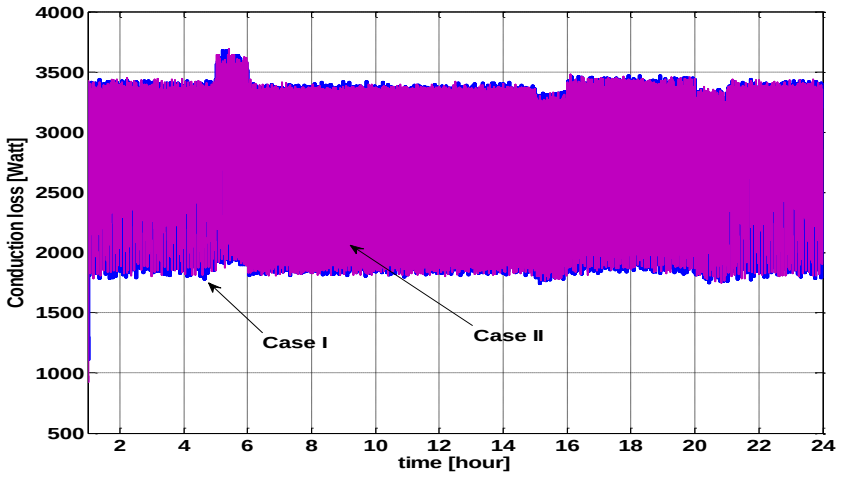

(b)

Fig. 7.10. GTO-based VSC, (a) Switching losses in cases I & II, (b) Conduction losses in cases I & II.

7.3. Optimal Power Flow Results

In order to verify the effectiveness of the proposed optimal voltage and power control in reducing the converter losses, GA-based OPF is determined for the model microgrid shown in Fig. 7. 11, and the results are compared with the regular power flow. The model microgrid consists of ten ac and dc buses interfaced using ten VSCs. The dc power is distributed among zonal loads through twelve dc cables. The per unit impedances of the

coupling transformer and dc cables are $0.1\,p.u.$ and $0.03\,p.u.$, respectively. Bus 1 is considered as the slack bus. Therefore, the VSC connected to it acts as the single voltage regulator. The generators are connected to buses 1, 3, 4 and 6, and consequently the VSCs that interface them with dc buses act as rectifiers. Two induction motors are connected to buses 2 and 5. Four ac zonal loads are fed from buses 7, 8, 9 and10. Therefore, the VSCs which supply the motors and the zonal loads act as inverters. Other data are shown directly in the figure.

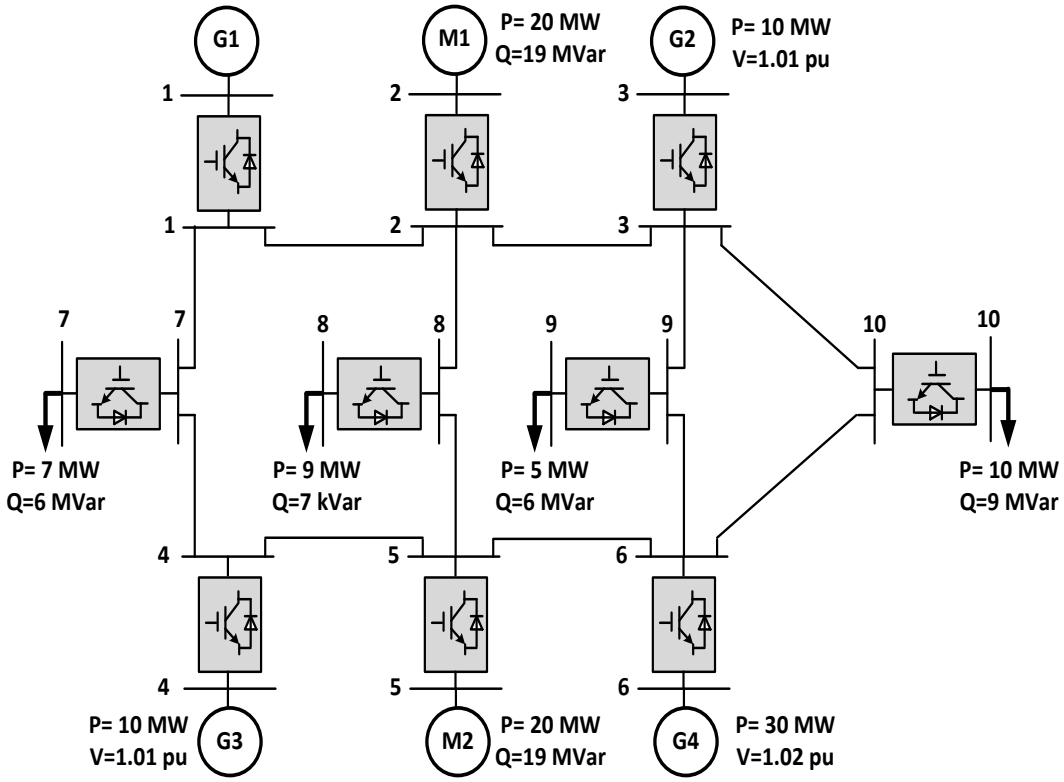

Fig. 7.11. Microgrid structure.

For the regular power flow, the voltage regulator was set to a fixed dc voltage of 1.05 p.u. The ac bus data and the VSC variables, including the converter losses, are shown in Tables V and VI, respectively. The base power was selected at 100 MVA. As seen, the demand at load buses is fully satisfied. In the second case, the optimum reference values of voltage for the voltage regulator, V_{dc_1}, VSC voltages, and ac bus voltages and powers produced by the generators were determined by the OPF. Tables VII and VIII list the ac bus data and the VSC variables, respectively, under the OPF condition. The ac bus voltages remain in the $0.95 - 1.05\,\mathrm{p.u.}$ range, and there is a balance between the generation and load at each bus. Comparing the VSCs dc voltage and modulation index values in Tables VI and VIII, it is demonstrated that in order to reduce the losses, the OPF selects the lowest possible dc voltage reference for the voltage regulator. Consequently, the modulation indices are at their maximum, to maintain the required voltage at VSCs terminals. Comparing the overall converter losses in both cases, it can be concluded that the GA-based OPF has reduced the losses from 10.1 MW to 4.2 MW while satisfying all the operational limits.

Table V

AC BUS DATA OF MICROGRID - REGULAR POWER FLOW

AC bus	**P**	**Q**	**V_m**
1	0.2123	0.2023	1.0000
2	-0.2000	-0.1900	0.9804
3	0.1000	0.1015	1.0100
4	0.1000	0.1015	1.0100
5	-0.2000	-0.1900	0.9804
6	0.3000	0.2084	1.0200
7	-0.0700	-0.0600	0.9939
8	-0.0900	-0.5415	0.9525
9	-0.0500	-0.0600	0.9940
10	-0.1000	-0.0900	0.9909

Table VI

CONVERTER DATA OF MICROGRID – REGULAR POWER FLOW

Converter	**V_{dc}**	**M**	**φ**	**Conduction Loss**	**Switching Loss**	**Converter Loss**
1	1.0500	0.9047	0.0217	0.4355	0.7761	1.2116
2	1.0457	0.9172	-0.0204	0.4039	0.7417	1.1456
3	1.0484	0.9157	0.0099	0.1136	0.3728	0.4864
4	1.0485	0.9156	0.0099	0.1136	0.3729	0.4865
5	1.0458	0.9172	-0.0204	0.4039	0.7418	1.1457
6	1.0503	0.9331	0.0294	0.6445	0.9482	1.5927
7	1.0482	0.9158	-0.0070	0.0550	0.2451	0.3001
8	1.0445	0.9191	-0.0095	1.5002	1.5335	3.0337
9	1.0486	0.9155	-0.0050	0.0412	0.2077	0.2489
10	1.0479	0.9161	-0.0101	0.1066	0.3587	0.4653
				Overall Losses=10.1 MW		

Table VII

AC BUS DATA OF MICROGRID - OPTIMAL POWER FLOW

AC bus	**P**	**Q**	**V_m**
1	0.2050	0.2021	1.0000
2	-0.2000	-0.1900	1.0132
3	0.1676	0.0001	1.0100
4	0.1678	0.0001	1.0100
5	-0.2000	-0.1900	1.0130
6	0.1718	0.0001	1.0200
7	-0.0700	-0.0600	1.0296
8	-0.0900	-0.0702	0.9525
9	-0.0500	-0.0600	1.0282
10	-0.1000	-0.0900	1.0245

Table VIII

CONVERTER DATA OF MICROGRID – OPTIMAL POWER FLOW

Converter	**V_{dc}**	**M**	**φ**	**Conduction Loss**	**Switching Loss**	**Converter Loss**
1	0.9800	0.9953	0.0209	0.42054	0.37619	0.79673
2	1.0322	1.0000	-0.0191	0.38125	0.35421	0.73546
3	1.0348	0.9762	0.0164	0.15740	0.21641	0.37381
4	1.0361	0.9749	0.0164	0.15768	0.21691	0.37459
5	1.0319	1.0000	-0.0191	0.38142	0.35421	0.73563
6	1.0348	0.9859	0.0165	0.16199	0.21973	0.38172
7	1.0354	1.0000	-0.0066	0.05201	0.116687	0.16888
8	1.0307	0.9817	-0.0101	0.08733	0.15737	0.2447
9	1.0341	1.0000	-0.0047	0.03905	0.09900	0.13805
10	1.0333	1.0000	-0.0094	0.10088	0.17104	0.27192
				Overall Losses= 4.2 MW		

Chapter 8

Conclusion & Future Work

A novel operating principle has been proposed for the autonomous microgrids. The flexible-voltage dc bus allows minimum-voltage operation whenever the full-load power is not needed. In turn, the minimum-voltage operation results in reduced switching losses, with no impact of the converter ratings and conduction losses. A method to calculate the minimum required dc-bus voltage was developed. The results of simulations of a 1.6 MW induction motor drive controlled with the proposed strategy have confirmed the effectiveness of the minimum-voltage operation in improving the efficiency of the system.

GA-based optimal power flow determination has been proposed for optimal dc voltage and power control in autonomous microgrids. MATLAB software package was used to develop the code for the optimization problem. Simulation results of a 20-bus microgrid model prove that the proposed method assigns the optimal voltage reference of the voltage regulator along with the optimal power references of the power dispatchers to minimize losses in power electronic converters. The proposed approach has successfully determined the optimal voltage and power references while satisfying the operational constraints and power balance. To verify the effectiveness of machine intelligence in reducing converter losses, the optimization results were compared with the results obtained from a conventional power flow solution. Radical reduction of losses has been demonstrated.

Future studies will involve an in-depth investigation of the issue of best combination

of single- and multi-input PECs, which is crucial for optimal design of microgrids. Judicious use of those PECs and the flexibility of voltage control will enhance the stability, reliability, responsiveness to changing operating conditions, compactness, and cost effectiveness of microgrids. Furthermore, voltage-power equations of these converters will be developed and embedded into power flow equations.

Different optimization techniques will be utilized to solve the optimization problem, and the results will be compared with the results in this dissertation. Multiple objectives such as minimizing distribution lines losses, emission level, and fuel consumption will also be taken into account. Multi-objective optimization algorithm will be employed to solve the new optimization problems.

References

[1] J. Rocabert, A. Luna, F. Blaabjerg, and P. Rodriguez, "Control of power converters in AC microgrids," *IEEE Trans. Power Electron*., vol. 27, no. 11, pp. 4734-4749, Nov. 2012.

[2] N. Hatziargyriou, "Microgrids," *IEEE Power and Energy Mag*., vol. 6, no. 3, pp. 26-29, 2008.

[3] G. Venkataramanan and C. Marnay, "A larger role for microgrids," *IEEE Power and Energy Mag*., vol. 6, no. 3, pp. 78-82, 2008.

[4] J. Driesen and F. Katiraei, "Design for distributed energy resources," *IEEE Power and Energy Mag*., vol. 6, no. 3, pp. 30-40, 2008.

[5] B. Kroposki et al., "Making microgrids work," *IEEE Power and Energy Mag*., vol. 6, no. 3, pp. 40-53, 2008.

[6] M. Olken. "Larger look at microgrids," *IEEE Power and Energy Mag*., vol. 6, no. 3, pp. 4-9, 2008.

[7] C. Marnay and G. Venkataramanan, "Microgrids in the evolving electricity generation and deliveryinfrastructure," *IEEE Power Engineering* Soc. Mtg, 2006.

[8] X. Liu and B. Su, "Microgrids – an integration of renewable energy technologies," *CICED'2008.*

[9] P. Asmuth and J. F. Verstege, "Optimal network structure for distribution systems with microgrids," *Intl. Conf. on Future Power Systems*, 2005.

[10] C. Marnay et al., "Policymaking for microgrids," *IEEE Power and Energy Mag*., vol. 6, no. 3, pp. 6-77, 2008.

[11] M. Barnes et al., "Real-world microgrids: An overview," *IEEE Intl. Conf. on Systems Engineering*, 2007.

[12] F. Katiraei et al., Microgrid management," *IEEE Power and Energy Mag*., vol. 6, no. 3, pp. 54-65, 2008.

[13] A. G. Tsikalakis and N. D. Hatziargyriou, "Centralized control for optimizing microgrid operation," *IEEE Trans. on Energy Conversion*, vol. 23, no. 1, pp. 241-248, 2008.

[14] A. L. Dimeas and N. D. Hatziargyriou, "A MAS architecture for microgrid control," *13th Intl. Conf. on Intelligent System Application to Power Systems*, 2005.

[15] Z. Jiang, "Agent-based control framework for distribute energy resources microgrids," *IEEE Intl. Conf. on Intelligent Agent Technology*, pp. 646-652, 2006.

[16] A. L. Dimeas and N. D. Hatziargyriou, "Operation of a multiagent system for microgrid control," *IEEE Trans. on Power Systems*, vol. 20, no. 3, pp. 1447-1455, 2005.

[17] A. L. Dimeas and N. D. Hatziargyriou, "Agent based control for microgrids," *IEEE Power Engineering Soc. Mtg*, 2007.

[18] S. J. Chatzivasiliadis et al., "Development of an agent based intelligent control for microgrids," *IEEE Power and Energy Soc. Mtg*., 2008.

[19] M. Bollen et al., "Performance indicators for microgrids during grid-connected and island operation," *IEEE Power Tech*, 2009.

[20] J. A. Pecas-Lopez et al., "Defining control strategies for analyzing microgrids' islanded operation," *IEEE Power Tech*, 2005.

[21] A. Salehi-Dobakshari et al., "Control of microgrids: Aspects and prospects," *Intl. Conf. on Networking, Sensing and Control*, pp. 38-43, 2011.

[22] Z. Jiang and X. Yu, "Power electronic interfaces for hybrid dc- and ac-linked microgrids," *Intl. Conf. on Networking, Sensing, and Control*, pp. 730-736, 2009.

[23] Z. Jiang and X. Yu, "Hybrid dc- and ac-linked microgrids: Towards integration of distributed energy resources," *Energy Conf*., 2008.

[24] P. Piagi and R. H. Lasseter, "Autonomous control of microgrids," *IEEE Power Engineering* Soc. Mtg, 2006.

[25] J. M. Guerrero et al., "Decentralized control for parallel operation of distributed generation inverters in microgrids using resistive output impedance," *IECON'2006*, pp. 5149-5154, 2006.

[26] C. K. Seo and P. W. Lehn, "Control and power management of converter fed microgrids," *IEEE Trans. on Power Systems*, vo. 23, no. 3, pp. 1088-1098, 2008.

[27] K. De Brabandere et al., "A voltage and frequency control method for parallel inverters," *IEEE Trans. on Power Electronics*," vol. 22, no. 4, pp. 1107-1115, 2007.

[28] J. A. Pecas-Lopez et al., "Control strategies for microgrids emergency operation," *Intl. Conf. on Future Power Systems*, 2005.

[29] I. A. Hiskens and E. M. Fleming, "Control of inverter-connected sources in autonomous microgrids," *ACC'2008*, pp. 586-590, 2008.

[30] T. C. Green and M. Prodanovic, "Control of inverter-based micro-grids," *Elsevier Electric Power Systems Research*, vol. 77, no. 9, pp. 1204-1213, 2007.

[31] H. Karimi, H. Nikkajoei, and R. Iravani, "Control of electronically-coupled distributed resource unit subsequent to an islanding event," *IEEE Trans. on Power Delivery*, vol. 23, no. 1, pp. 493-501, 2008.

[32] I. J. Balaguer et al., "Intelligent control for intentional islanding operation of microgrids," *IEEE Intl. Conf. on Sustainable Energy Technologies*, pp. 898-9003, 2008.

[33] T. Thacker et al., "Islanding detection using a coordinate transformation based phase-locked loop," *PESC'2007*, pp. 1151-1156, 2007.

[34] C. K. Sao and P. W. Lehn, "Intentional islanded operation of converter fed microgrids," *IEEE Power Engineering Soc. Mtg*, 2006.

[35] A. Llaria et al., "Survey on miscrogrids: Analysis of technical limitations to carry out new solutions," *European Conf. on Power Electronics and Applications*, 2009.

[36] S. Bala and G. Venkataramanan, "Autonomous power electronic interfaces between microgrids," *IEEE Energy Conversion Congr. and Exp.*, pp. 3006-3013, 2009.

[37] I. Serban and C. Marinescu, "A new control method for power quality improvement in island microgrids," *IEEE Intl. Symp. on Industrial Electronics*, pp. 2258-2263, 2008.

[38] T. Tanabe et al., "Optimized operation and stabilization of microgrids with multiple energy resources," *Intl. Conf. on Power Electronics*, pp. 74-78, 2007.

[39] T. Tanabe et al., An active network control method using distributed energy resources in microgrids," *Power Electronics and Motion Control Conf*., pp. 2478-2480, 2008.

[40] S. M. Bathaee and M. H. Abdollahi, "Fuzzy-nural controller design for stability enhancement of microgrids," *Intl. Universities Power Engineering Conf*., pp. 562-569, 2007.

[41] M. H. Abdollahi and S. M. Bathaee, "Sliding mode controller for stability enhancement of microgrids," *IEEE Transmission and Distribution Conf. and Exp*., 2008.

[42] K. De Brabandere et al., "Control of microgrids," *IEEE Power Engineering Soc. Mtg*, 2007.

[43] Y. Zhu, Z. Yin, and J. Tian, "Microgrids based on dc energy pool," *Energy Conf*., 2008.

[44] D. J. Cox and T. Davis, "Distributed generation and sensing for intelligent distributed microgrids," *IEEE Intl. Conf. on Systems Engineering*, 2006.

[45] J. C. Vasquez et al., "Hierarchical control of intelligent microgrids," *IEEE Industrial Electronics Mag*., vol. 4, no. 4, pp. 23-29, 2010.

[46] R. H. Lasseter, "Smart distribution: Coupled microgrids," *Proc.of the IEEE*, vol. 99, no. 6, pp. 1074-1082, 2011.

[47] A. S. Dobakhshari, S. Azizi, and A. M. Ranjbar, "Control of microgrids: Aspects and Prospects," *Intl. Conf. on Networking, Sensing and Control*, pp. 38-43, 2011.

[48] S. X. Chen and H. B. Gooi, "Sizing of energy storage system for microgrids," *Intl. Conf. on* Probabilistic *Methods Applied to Power Systems*, pp. 6-11, 2010.

[49] H. J. Laaksonen, "Protection principles for future microgrids," *IEEE Trans. on Power Electronics*, vol. 25, no. 12, pp. 2910-2918, 2010.

[50] D. Pudjianto et al., "Investigation of regulatory, commercial, economic and environmental issues in microgrids," *Intl. Conf. on Future Power Systems*, 2005.

[51] T. Feehally and M. Barnes, "Reducing the cost of domestic microgrids," *Intl. Conf. on Electrical Machines and Drives*, 2010.

[52] A. Prasai et al., "Minimizing emissions in microgrids while meeting reliability and power quality objectives," *Intl. Power Electronics Conf*., 2010.

[53] A. Krkoleva et al., "Social aspects of wider microgrids deployment," *Mediterranean Conf. and Exhib. On Power Generation, Transmission, Distribution and Energy Conversion*, 2010.

[54] T. L. Vandoorn et al., "A control strategy for islanded microgrids with dc-link voltage control," *IEEE Trans. on Power Delivery*, vol. 26, no. 2, pp. 703-713, 2011.

[55] T. L. Vandoorn et al., "Power balancing in islanded microgrids by using a dc-bus voltage reference," *Intl. Symp. on Power Electronics, Electrical Drives, Automation and Motion*, pp. 884-889, 2010.

[56] S. Anand and B. G. Fernandes, "Optimal voltage level for dc microgrids," *IECON'2010*, pp. 3034-3039.

[57] R. Martinez-Cid and E. O'Neill-Carrillo, "Sustainable microgrids for isolated systems," *Transmission and Distribution Conf. and Exp.*, 2010.

[58] B. Wu, Y. Lang, N. Zrgari, and S. Kouro, *Power Conversion and Control of Wind Energy Systems*, J. Wiley, 2011.

[59] B. Kroposki, et al. "Benefits of power electronic interfaces for distributed energy systems," IEEE Trans. Energy Conversion, vol. 25, no. 3, pp. 901-908, Sep. 2010.

[60] http://www.renewableenergyworld.com/rea/home

[61] P. rodriguez, A. Timbus, R. Teodorescu, M. Liserre, and F. Blaabjerg, "Reactive power control for improving wind turbine system behavior under grid faults," *IEEE Trans. Power Electron*., vol. 24, no. 7, pp. 1798-1801, Jul. 2009.

[62] J. C. Vasquez, J. M. Guerrero, A. Luna, P. Rodriguez, and R. Teodorescu, "Adaptive droop control applied to voltage-source inverters operating in grid-connected and islanded modes," *IEEE Trans. Ind. Electron.*, vol. 56, no. 10, pp. 4088-4096, Oct. 2009.

[63] H. Laaksonen, P. Saari, and R. Komulainen, "Voltage and frequency control of inverter based weak LV network microgrid," in *Proc. Int. Conf. Future Power Syst.*, 2005, pp. 1–6.

[64] K. De Brabandere, B. Bolsens, J. Van den Keybus, A. Woyte, J. Driesen, and R. Belmans, "A voltage and frequency droop control method for parallel inverters," *IEEE Trans. Power Electron.*, vol. 22, no. 4, pp. 1107–1115, Jul. 2007.

[65] S. J. Chiang, C. Y. Yen, and K. T. Chang, "A multimodule parallelable series-connected PWM voltage regulator," *IEEE Trans. Ind. Electron.*, vol. 48, no. 3, pp. 506–516, Jun. 2001.

[66] Y. Xiaoxiao, A. M. Khambadkone, W. Huanhuan, and S. Terence, "Control of parallel-connected power converters for low-voltage microgrid—Part I: A hybrid control architecture," *IEEE Trans. Power Electron.*, vol. 25, no. 12, pp. 2962–2970, Dec. 2010.

[67] IEEE Std. 1709-2010: "IEEE recommended practice for 1 to 35 kV medium voltage DC power systems on ships," DC Power Systems on Ships Working Group of the IEEE Industry Applications Society Petroleum & Chemical Industry (IAS/PCI) Committee, 2010.

[68] S. Bose, S. Pal, B. Natarajan, C. M. Scoglio, S. Das and N. N. Schulz, "Analysis of optimal reconfiguration of shipboard power systems," *IEEE Trans. on Power Systems*, vol. 27, no. 1, pp. 189-197, Feb. 2012.

[69] J. G. Ciezki, and R. W. Ashton, "Selection and stability noues associated with a navy shipboard dc zonal electric distribution system," *IEEE Trans. on Power Delivery*, vol. 15, no. 2, pp. 665-669, Apr. 2000.

[70] F. D. Kanellos, G. J. Tsekouras, J. Prousalidis, and I. K. Hatzilau, "Effort to formulate voltage modulation constraints in ship-electrical systems with pulsed loads,"*IET Electr. Syst. Transp.*, vol. 2., no. 1, pp. 18-28, Jan. 2012.

[71] F. D. Kanellos, G. J. Tsekouras, J. Prousalidis, and I. K. Hatzilau, "An effort to formulate frequency modulation constraints in ship-electrical systems with pulsed loads,"*IET Electr. Syst. Transp.*, vol. 1., no. 1, pp. 11-23, Jan. 2011.

[72] X. Feng, K. L. Butler-Purry, and T. Zourntos, "Multi-agent system-based real-time load management for all-electric ship power systems in dc zone level," *IEEE Trans. on Power Systems*, vol. 27, no. 4, pp. 1719-1728, Nov. 2012.

[73] G. Seenumani, J. Sun and H. Peng, "Real-time power management of integrated power systems in all electric ships leveraging multi time scale property," *IEEE Trans. on Control Systems Technology*, vol. 20, no. 1, pp. 232-240, Jan. 2012.

[74] V. Arcidiacono, A. Monti, and G. Sulligoi, "Generation control system for improving design and stability of medium-voltage DC power systems on ships,"*IET Electr. Syst. Transp.*, vol. 2., no. 3, pp. 158-167, Apr. 2012.

[75] S. Yeleti, and Y. Fu, "Load flow and security assessment of VSC based MVDC shipboard power systems," *NAPS* 2011.

[76] P. Kankanala, S. C. Srivastava, A. K. Srivastava, and N. Schulz, "Optimal control of voltage and power in a multi-zonal MVDC shipboard power system," *IEEE Trans. on Power Systems*, vol. 27, no. 2, pp. 642-650, May 2012.

[77] J. Kedariseti and P. Mutschler, "A motor-friendly quasi-resonant DC-link inverter with lossless variable zero-voltage duration," *IEEE Trans. on Power Electronics*, vol. 27, no. 5, pp. 2613-2622, May 2012.

[78] B. Lin, and P. Cheng, "New ZVS DC-DC converter with series-connected transformers to balance output currents," *IEEE Trans. on Power Electronics*, vol. 29, no. 1, pp. 246-255, Jan. 2014.

[79] E. Chu, M. Wu, L. Huang, X. hou, and H. Zhang, "Research on a novel modulation strategy for auxiliary resonant commutated pole inverter with the smallest loss in auxiliary commutation circuits," *IEEE Trans. on Power Electronics*, vol. 29, no. 3, pp. 1103-1117, Mar. 2014.

[80] R. Li, Z. Ma, and D. Xu, "A ZVS grid-connected three-phase inverter," *IEEE Trans. on Power Electronics*, vol. 27, no. 8, pp. 3595-3604, Aug. 2012.

[81] Q. Lei, D. Cao, and F. Peng, "Novel loss and harmonic minimized vector modulation for a current-fed quasi-Z-source inverter in HEV motor drive application," *IEEE Trans. on Power Electronics*, vol. 29, no. 3, pp. 1344-1357, Mar. 2014.

[82] A. Q. Huang, and B. Zhang, "Comparing SiC switching power devices: MOSFET, NPN transistor and GTO thyristor," Solid-State electronics, vol. 4, pp. 325-340, 2000.

[83] M. S. Chinthavali, L . M. Tolbert, and B. Ozpineci, "4H-SiC GTO thyristor and p-n diode loss models for HVDC converter," in *Proc. IEEE Ind. Appl. Conf.,* pp. 1238-1243, 2004.

[84] M. H. Bierhoff and F. W. Fuchs, "Semiconductor losses in voltage source and current source IGBT converters based on analytical derivation," in *Proc. IEEEPower Electronics Specialists Conf. PESC'*2004, pp. 2836-2842.

[85] F. Blaabjerg, J. Pederson, S. Sigurjonsson, and A. Elkjaer, "An extended model of power losses in hard-switched IGBT-inverters," in *Proc. IEEE Ind. Appl. Conf.,* pp. 1454-1463, 1996.

[86] D. Graovac and M. Purscvhel, "IGBT power losses calculation using the datasheet parameters," Application Note, Infineon, Jan. 2009.

[87] X. Lei, L. Yongdong, W. Kui, J. Clare, and P. Wheeler, "Research on the amplitude coefficient for multilevel matrix converter space vector modulation," *IEEE Trans. on Power Elec.*, vol. 27, no. 8, pp.3544-3556, Aug. 2012.

[88] M. Farasat and E. Karaman, "Efficiency-optimized hybrid field oriented and direct torque control of induction motor drive," in *Proc. Intl.Conf. on Electrical Machines and Systems ICEMS'2011*, pp. 1-4.

[89] C. Yu, J. Tamura, and R. Lorenz, "Optimum Dc bus voltage analysis and calculation method for inverters/motors with variable dc bus voltage," *IEEE Trans. on Ind. Appl.*, vol. 49, no. 6, pp.2619-2627, Nov./Dec. 2013.

[90] M. Farasat, A. Arabali and A. M. Trzynadlowski, "A novel control principle for all-electric ship power systems," in *Proc. IEEE Electric Ship Technologies Symp.*, pp. 178-184, Apr. 2013.

[91] K. S. Pandya, S. K. Joshi, "A survey of optimal power flow methods," *Journal of Theoretical and Applied Information Technology*, pp. 450-458, 2008.

[92] T. S. Chung and Ge Shaoyun, "A recursive LP-based approach for optimal capacitor allocation with cost-benefit consideration", *Electric Power Syst. Research,* vol. 39, pp. 129-136, 1997.

[93] E. Lobato, L. Rouco, M. I. Navarrete, R. Casanova and G. Lopez, "An LP-based optimal power flow for transmission losses and generator reactive margins minimization", in *Proc. of IEEE porto power tech conference*, Portugal, Sept. 2001.

[94] F. G. M. Lima, F. D. Galiana, I. Kockar and J. Munoz, "Phase shifter placement in large scale systems via mixed integer linear programming", *IEEE Trans. Power Syst,* vol. 18, no. 3, pp. 1029-1034, Aug. 2003.

[95] S. D. Chen and J. F. Chen, "A new algorithm based on the Newton-Raphson approach for real-time emission dispatch", *Electric Power Syst. Research,* vol. 40, pp. 137-141, 1997.

[96] K. L. Lo and Z. J. Meng, "Newton-like method for line outage simulation", *IEE proc.- Gener. Transm. Distrib.*, vol. 151, no. 2, pp. 225-231, March 2004.

[97] X. Tong and M. Lin, "Semi-smooth Newton-type algorithms for solving optimal power flow problems", in *Proc. of IEEE/PES Transmission and Distribution Conference,* Dalian, China, 2005, pp.1-7.

[98] J. A. Momoh, "*A generalized quadratic-based model for optimal power flow*", pp. 261- 267.

[99] X. Lin, A. K. David and C. W. Yu, "Reactive power optimization with voltage stability consideration in power market systems", *IEE proc.-Gener. Transm. Distrib.,* vol. 150, no. 3, pp. 305-310, May 2003.

[100] A. berizzi, M. Delfanti, P. Marannino, M. S. Pasquadibisceglie and A. Silvestri, "Enhanced security-constrained OPF with FACTS devices", *IEEE Trans. Power Syst.,* vol. 20, no. 3, pp. 1597-1605, Aug. 2005.

[101] J. A. Momoh and J. Zhu, "Multi-area power systems economic dispatch using nonlinear convex network flow programming", *Electric Power Syst. Research,* vol. 59, pp. 13-20, 2001.

[102] D. Pudjianto, S. Ahmed and G. Strbac, "Allocation of VAR support using LP and NLP based optimal power flows", *IEE proc.- Gener. Transm. Distrib.*, vol. 149, no. 4, pp. 377-383, July 2002.

[103] G. L. Torres and V. H. Quintana, "A jacobian smoothing nonlinear complementarity method for solving nonlinear optimal power flows", in *Proc. Of 14th PSCC,* Sevilla, Session 41, paper 1, June 2002, pp.1-7.

[104] A. K. Sharma, "Optimal number and location of TCSC and loadability enhancement in deregulated electricity markets using MINLP", *Int. J. of Emerging Electric Power Syst.,* vol. 5, issue. 1, pp. 1-13, 2006.

[105] Badrul H. Chowdhury, "Towards the concept of integrated security: optimal dispatch under static and dynamic security constraints", *Electric Power Syst. Research*, vol.25, pp. 213-225, 1992.

[106] N. Iwan Santoso and Owen T. Tan, "Neuralnet based real time control of capacitors installed on distribution systems", *IEEE Trans. Power delivery,* vol.5, no.1, pp. 266- 272, Jan. 1990.

[107] V. Miranda and J. T. Saraiva, "Fuzzy modeling of power system optimal load flow", *IEEE Trans. Power Syst.,* vol. 7, no. 2, pp.843-849, 1992.

[108] V. C. Ramesh and Xuan Li, "A fuzzy multi-objective approach to contingency constrained OPF", *IEEE Trans. Power Syst.,* vol. 12, no. 3, pp.1348-1354, Aug. 1997.

[109] Narayana Prasad Padhy, "Congestion management under deregulated fuzzy environment", *IEEE International Conference on Electric Utility Deregulation, Restructuring and Power Technologies*, pp. 133-139. April 2004.

[110] I. K. Yu and Y. H. Song, "A novel short-term generation scheduling technique of thermal units using ant colony search algorithms", *Electrical power and energy syst.,* vol. 23, pp. 471-479, 2001.

[111] Libao Shi, Jin Hao, Jiaqi Zhou and Guoyu Xu, "Ant colony optimization algorithm with random perturbation behavior to the problem of optimal unit commitment with probabilistic spinning reserve determination", *Electric Power Syst. Research*, vol. 69, pp. 295-303, 2004.

[112] R. Meziane, Y. Massim, A. Zeblah, A. Ghoraf and R. Rahli, "Reliability optimization using ant colony algorithm under performance and cost constraints", *Electric Power Syst. Research*, vol. 76, pp. 1-8, 2005.

[113] H. Yoshida, K. Kawata, Y. Fukuyama et al. "A particle swarm optimization for reactive power and voltage control considering voltage security assessment", *IEEE Trans. Power Syst.*, vol. 15, no. 4, pp. 1232-1239, Nov. 2000.

[114] J. B. Park, Ki. S. Lee, J. R. Shi and K. Y. Lee, "A particle swarm optimization for economic dispatch with non-smooth cost functions", *IEEE Trans. Power Syst.*, vol. 20, no. 1, pp. 34-42, Feb. 2005.

[115] Cui-Ru Wang, He-Jin Yuan, Zhi-Qiang Huang, Jiang-Wei Zhang and Chen-Jun Sun, "A modified particle swarm optimization algorithm and its application in optimal power flow problem", in *4th International Conference on Machine Learning and Cybernetics*, pp.2885-2889, August 2005.

[116] J. G. Vlachogiannis and K. Y. Lee, "Determining generator contributions to transmission system using parallel vector evaluated particle swarm optimization", *IEEE Trans. Power Syst.*, vol.20, no.4, pp.1765- 1774, Nov. 2005.

[117] M. Saravanan, S. M. R. Slochanal, P. Venkatesh, J. P. S. Abraham, "Application of particle swarm optimization technique for optimal location of FACTS devices considering cost of installation and system loadability", *Electric Power Syst. Research*, vol. 77, pp. 276-283, 2007.

[118] P. H. Chen and H. C. Chang, "Large scale economic dispatch by genetic algorithm", *IEEE Trans. Power Syst.*, vol. 10, no. 4, pp. 1919-1926, Nov. 1995.

[119] T. S. Chung and Y. Z. Li, "A hybrid GA approach for OPF with consideration of FACTS devices", *IEEE Power Engineering Review*, pp. 47-50, Feb. 2001.

[120] L. J. Cai, I. Erlich and G. Stamtsis, "Optimal choice and allocation of FACTS devices in deregulated electricity market using genetic algorithms", *IEEE PES*, 2004.